

REVIEW ARTICLE

Modeling Dislocations at Different Scales

Yang Xiang*

*Department of Mathematics, Hong Kong University of Science and Technology,
Clear Water Bay, Kowloon, Hong Kong.*

Received 27 October 2005; Accepted (in revised version) 13 January 2006

Communicated by Weinan E

Abstract. In this article, we give an introduction to the basic theory of dislocations and some dislocation models at different length scales. Dislocations are line defects in crystals. The continuum theory of dislocations works well at the length scale of several lattice constants away from the dislocations. In the region surrounding the dislocations (core region), the crystal lattice is heavily distorted, and atomistic models are used to describe the atomic arrangement and related properties. The Peierls-Nabarro models of dislocations incorporate the atomic features into the continuum theory, therefore provide an alternative way to understand the dislocation core properties. The numerical simulation of the collective motion and interactions of dislocations, known as dislocation dynamics, is becoming a more and more important tool for the investigation of the plastic behaviors of materials. Several simulation methods for dislocation dynamics are also reviewed in this article.

Key words: Dislocations; modeling; dislocation dynamics; Peierls-Nabarro model.

Contents

1	Introduction	384
2	Continuum theory	389
3	Dislocations in crystals: atomistic models	394
4	The Peierls-Nabarro model	400
5	Dislocation dynamics	408
6	Level set method for dislocation dynamics	411

*Correspondence to: Yang Xiang, Department of Mathematics, Hong Kong University of Science and Technology, Clear Water Bay, Kowloon, Hong Kong. Email: maxiang@ust.hk

1 Introduction

Dislocations are line defects in crystals. The dislocation theory had its origins in the early years of the last century [1–4], and has been an active research area ever since [5–7]. The dislocation theory is essential for the understanding of the plastic deformation (permanent deformation) properties of crystals. In this article, we shall briefly review the basic dislocation theory and some dislocation models at different length scales.

We first review the basic properties of dislocations. Fig. 1(a) shows the geometry of one type of dislocations: edge dislocations, in a simple cubic lattice, where the atomic arrangement is uniform in the direction perpendicular to the paper. An edge dislocation can be imagined as being formed by inserting an extra half plane of atoms into a perfect crystal, see Fig. 1(b). The boundary of the extra half plane, where the lattice is heavily distorted, is the edge dislocation. An edge dislocation can also be imagined as being formed by making a cut in a perfect crystal, and shifting the atoms on one side of the cut relative to those on the other side by one lattice spacing, in a direction in the cut plane and perpendicular to the cut boundary line, see Fig. 1(c). The boundary line of the cut is the edge dislocation. Note that the cut in the latter process is perpendicular to the extra half plane of atoms in the former one. Both processes give the same atomic arrangement for an edge dislocation. Fig. 2 shows the geometry of another type of dislocations: screw dislocations, in a simple cubic lattice. A screw dislocation can be imagined as being formed by shifting the atoms on one side of a half plane relative to the atoms on the other side by one lattice constant, in a direction parallel to the boundary of the half plane. The boundary of the half plane is the screw dislocation.

The motion of dislocations leads to plastic deformation in crystals. When single crystals are stressed, they undergo plastic deformation when the stress is high enough. However, the critical stress in a real material is several orders of magnitude lower than the theoretical stress to shear a perfect crystal [8]. Taylor [2], Orowan [3] and Polanyi [4] first pointed out that dislocations are responsible for this low critical stress. A simple demonstration is given in Fig. 3. In Fig. 3, a single crystal containing an edge dislocation is shown. The edge dislocation is perpendicular to the paper and the atomic arrangement is uniform in this direction. Away from the edge dislocation, the atomic arrangement is close to that in a perfect crystal; while near the dislocation, the lattice is heavily distorted. Under an applied shear stress, near the dislocation, the bond between atoms A and C forms and the bond between atoms B and C breaks, see Fig. 3(a) and (b). In this way, the edge dislocation moves a distance of one lattice spacing. This process repeats under the applied stress. When the dislocation moves to the crystal boundary, a step is produced there and the crystal undergoes a plastic (permanent) deformation, see Fig. 3(c). The shear stress required in this process is much lower than that to shift a perfect crystal.

Burgers vector [9] is used to characterize a dislocation. First, the direction of the dislocation needs to be defined, which is the direction of the unit tangent vector of the dislocation. Consider a closed loop enclosing an edge dislocation, see Fig. 4(a). The edge dislocation is perpendicular to the paper, and the extra half plane of atoms are

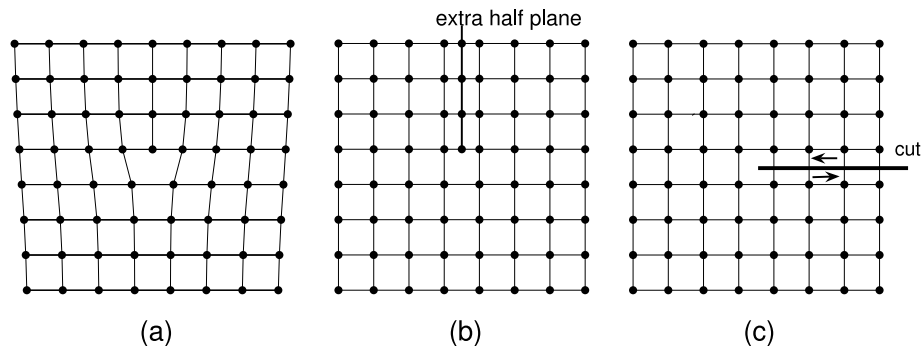


Figure 1: Geometry of an edge dislocation. (a) An edge dislocation. The atomic arrangement is uniform in the direction perpendicular to the paper. (b) The edge dislocation can be imagined as being formed by inserting an extra half plane of atoms into a perfect crystal. (c) It can also be imagined as being formed by making a cut in a perfect crystal, and shifting the atoms on one side of the cut relative to those on the other side by one lattice spacing.

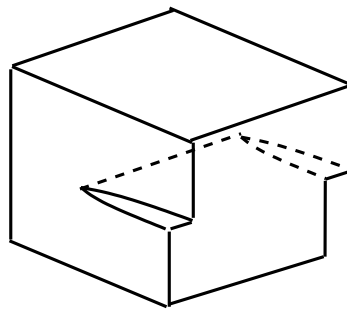


Figure 2: Geometry of a screw dislocation. A screw dislocation can be imagined as being formed by shifting the atoms on one side of a half plane relative to the atoms on the other side by one lattice constant, in a direction parallel to the boundary of the half plane.

above the edge dislocation. The closed loop enclosing the dislocation, which is called the Burgers circuit of the dislocation, is in a right-hand sense with respect to the direction of the dislocation. Assuming that the direction of this edge dislocation is pointing out of the paper, the Burgers circuit is counterclockwise. If we put this circuit with the same atom-to-atom sequence in a perfect crystal, it is not closed, see Fig. 4(b). The vector required to close this circuit is the Burgers vector of this dislocation, denoted by \mathbf{b} . For an edge dislocation, its Burgers vector is perpendicular to itself. In the first imagined process to form the edge dislocation, see Fig. 1(b), the Burgers vector is the lattice vector perpendicular to the extra half plane of atoms. In the second imagined process to form the edge dislocation, see Fig. 1(c), the atoms on one side of the cut are displaced relative to those on the other side by the amount of a Burgers vector in the cut plane.

If we assign an opposite line direction to the dislocation, i.e., assume that the direction of the edge dislocation is pointing into the paper in Fig. 4, the Burgers vector also changes to its opposite direction. There is no general agreement in the literature on the convention

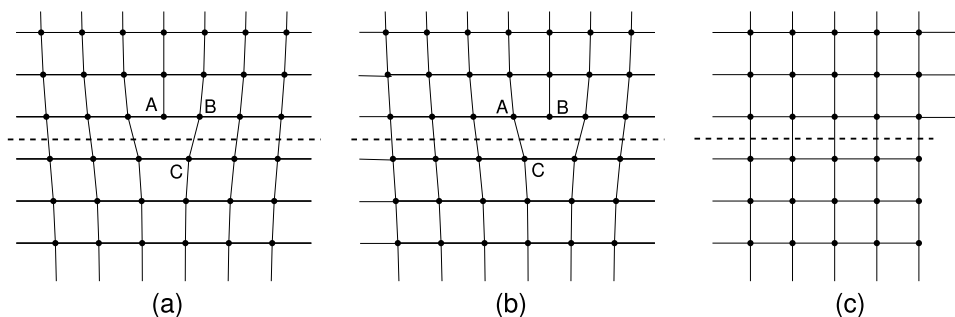


Figure 3: Motion of an edge dislocation (this motion is called glide): (a) An edge dislocation. (b) Under an applied shear stress, the bond between atoms A and C forms and the bond between atoms B and C breaks. As a result, the edge dislocation moves one lattice spacing to the right. (c) When the dislocation moves to the crystal boundary, a step is produced.

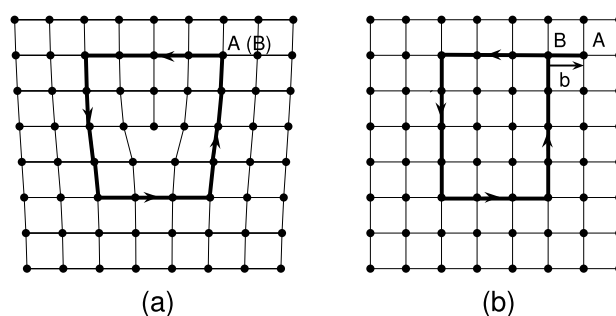


Figure 4: Definition of the Burgers vector. (a) A closed loop enclosing an edge dislocation (Burgers circuit of an edge dislocation). The starting point A and the ending point B of the loop coincide. (b) The same Burgers circuit in a perfect crystal. The starting point A and the ending point B of the circuit do not coincide. The vector required to close the circuit is the Burgers vector \mathbf{b} .

for the direction of the Burgers vector of the edge dislocation with this atomic arrangement, e.g., in books [5, 12, 14], the former definition is used; while in books [6, 13], the latter is used. In either convention, the edge dislocation whose extra half plane of atoms are above the dislocation is denoted by \perp , and the edge dislocation with an extra half plane of atoms below the dislocation has a Burgers vector with opposite sign, denoted by \top .

We have seen that for an edge dislocation, its Burgers vector is perpendicular to its line direction. For a screw dislocation, its Burgers vector is parallel to its line direction. In a general case, the dislocation line may have an arbitrary angle to its Burgers vector, usually with a mixed character of edge and screw. Fig. 5 shows a circular dislocation loop in a plane that also contains the Burgers vector. At points A and B, the dislocation is pure edge and at points C and D, it is pure screw. At any other point, say point E, the dislocation is mixed type.

The Burgers vector is a constant vector along a dislocation line. The dislocation lines can end at the boundary of a single crystal, but cannot end inside. Inside a crystal, they can either form loops or end at dislocation nodes, where three or more dislocation lines

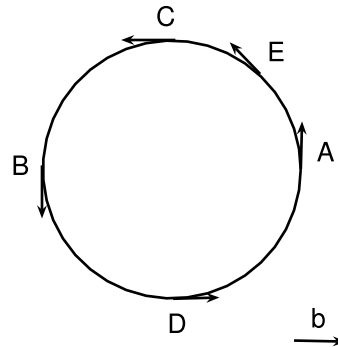


Figure 5: A dislocation loop. At point A or B, the dislocation is pure edge, and at point C or D, it is pure screw. At point E, the dislocation is mixed type.

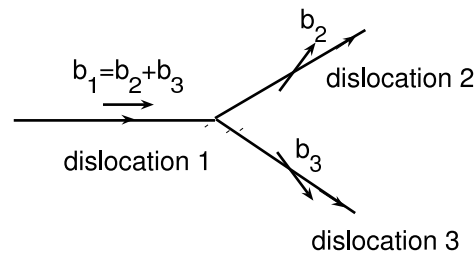


Figure 6: A dislocation node.

meet. Fig. 6 shows a node where dislocation 1 (with Burgers vector \mathbf{b}_1) is splitted into dislocations 2 (with Burgers vector \mathbf{b}_2) and 3 (with Burgers vector \mathbf{b}_3). It is required that $\mathbf{b}_1 = \mathbf{b}_2 + \mathbf{b}_3$. This is the conservation of Burgers vectors. Generally, at a node where n dislocations meet, if all the dislocations are pointing into the node, then we have $\sum_{i=1}^n \mathbf{b}_i = 0$, where \mathbf{b}_i is the Burgers vector of the i -th dislocation.

The energy per unit length of a dislocation can be approximately written as $\alpha G b^2$ (see the next section), where b is the length of its Burgers vector, G is the shear modulus, and α is a constant depending on the angle between the dislocation line direction and its Burgers vector. If we assume that the constant is the same for all dislocations, then we have a simple rule for the reaction of dislocations, which is the Frank's rule [10]. Consider two dislocations with Burgers vectors \mathbf{b}_2 and \mathbf{b}_3 , respectively. The total energy of these two dislocations is $\alpha G (b_2^2 + b_3^2)$. If they react to form one single dislocation with Burgers vector $\mathbf{b}_1 = \mathbf{b}_2 + \mathbf{b}_3$, then the energy is $\alpha G b_1^2$. So when $b_1^2 < b_2^2 + b_3^2$, the combined single dislocation has lower energy thus the reaction is favorable. Otherwise the reaction is unfavorable. In crystals, when the Burgers vector of a dislocation is a lattice vector, the dislocation is called a perfect dislocation. The possible Burgers vectors for perfect dislocations are the shortest lattice vectors, because otherwise a dislocation can dissociate into two dislocations with shorter Burgers vectors and lower energy. Sometimes, non-perfect dislocations (partial dislocations) that have non-lattice-vector Burgers vectors may also be energetically stable, for example, in the face-centered cubic crystals. This will

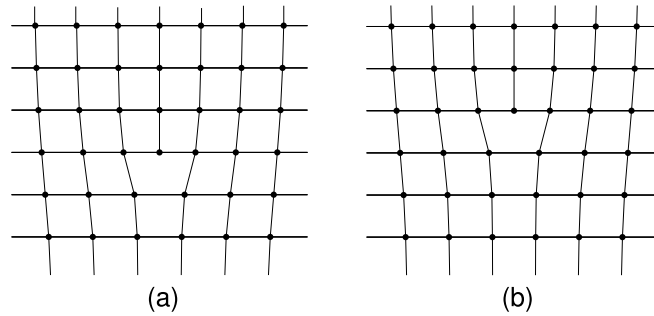


Figure 7: Dislocation climb. (a) An edge dislocation. (b) The edge dislocation climbs up by one lattice spacing. One line of atoms (perpendicular to the paper) have been removed.

be discussed in Section 3.

As described previously, an edge dislocation can move under an applied stress in a plane containing its Burgers vector and itself, see Fig. 3. The dash line in Fig. 3 shows the position of this plane, which is perpendicular to the extra half plane of atoms in the first imagined method to form the edge dislocation. In the second imagined method to form the edge dislocation, this plane contains the cut where the atoms on one side are displaced relative to those on the other side by the amount of the Burgers vector; moreover, since the edge dislocation is the boundary of the cut, the cut area changes as the dislocation moves. This plane containing the dislocation and its Burgers vector is the slip plane of the dislocation, and the motion of the dislocation in the slip plane is called glide. If we want to move an edge dislocation in the direction perpendicular to the slip plane, we need to add or remove lines of atoms near the dislocation, see Fig. 7. This motion of dislocation is called climb. For this reason, the dislocation glide is referred to as the conservative motion and the dislocation climb is referred to as the non-conservative motion. The addition or removal of atoms required in the dislocation climb is manifested by the diffusion process of atoms, therefore climb is very difficult except at high temperatures. The screw dislocation is special because its Burgers vector is parallel to itself, so the slip plane is not well-defined, and it can move in any plane containing itself without addition or removal of atoms. In real crystals, the possible slip planes of dislocations are the close-packed planes in which dislocations are easy to move (see Section 4). Screw dislocations also tend to move in these planes, and sometimes may move from one such plane to another, which is known as cross-slip.

The dislocations occur in all crystals. The density of dislocations is defined as the total length of dislocations per unit volume. In a well-annealed metal (anneal is a heat treatment to remove defects in crystals), the dislocation density is low and is typically about $10^6 \sim 10^8/\text{cm}^2$. After plastic straining, the dislocation density increases and may attain values about $10^{10} \sim 10^{11}/\text{cm}^2$. There are many reasons for the fact that dislocations occur in all crystals, for example, the nucleation of dislocations due to the internal stress generated by impurities or thermal gradients. Besides, dislocations also help the growth of the crystals, remaining in the crystals and extending as the crystals grow. The observation that the

dislocation density increases after plastic straining seems to contradict the fact that the dislocations move to the surface of the crystal in the plastic flow under an applied stress, see Fig. 3. This increase of the dislocation density is due to the dislocation multiplication during the plastic deformation process. There are many mechanisms for the dislocation multiplication, one is the Frank-Read source [11] (See Section 6 for a simulation result).

More on dislocations can be found in many classical and introductory books, for example, [5–7, 12–15].

2 Continuum theory

We now briefly review the continuum theory of dislocations based on the linear elasticity theory. In the continuum theory, a dislocation is considered as a line in a continuous medium, while the details of the atomic structure are neglected. At the length scale of several lattice constants away from the dislocation, the strain and stress field are described well by the continuum dislocation theory. More on the continuum theory of dislocations can be found in, e.g., [5, 6, 14, 15].

In the continuum theory, within the body containing the dislocations, the elastic displacement vector is increased by the amount of the Burgers vector along any loop enclosing the dislocation, i.e.,

$$\oint_L d\mathbf{u} = \mathbf{b}, \quad (2.1)$$

where \mathbf{u} is the elastic displacement vector, \mathbf{b} is the Burgers vector of the dislocation, L is any contour enclosing the dislocation line. Eq. (2.1) can be rewritten in terms of the distortion tensor \mathbf{w} , $w_{ij} = \partial u_j / \partial x_i$ for $i, j = 1, 2, 3$, as

$$\nabla \times \mathbf{w} = \xi \delta(\gamma) \otimes \mathbf{b}, \quad (2.2)$$

where ξ is the unit vector tangent to the dislocation line, $\delta(\gamma)$ is the two dimensional delta function in the plane perpendicular to the dislocation, and the operator \otimes computes the tensor product of two vectors.

In the linear elasticity theory, the strain tensor is defined as

$$\epsilon_{ij} = \frac{1}{2}(w_{ij} + w_{ji}) \quad (2.3)$$

for $i, j = 1, 2, 3$. The stress tensor σ is determined from the strain tensor by the linear elastic constitutive equations (Hooke's law)

$$\sigma_{ij} = \sum_{k,l=1}^3 C_{ijkl} \epsilon_{kl} \quad (2.4)$$

for $i, j = 1, 2, 3$, where $\{C_{ijkl}\}$ is the elastic constant tensor. For an isotropic medium, the constitutive equations can be written as

$$\sigma_{ij} = 2G\epsilon_{ij} + G\frac{2\nu}{1-2\nu}(\epsilon_{11} + \epsilon_{22} + \epsilon_{33})\delta_{ij} \quad (2.5)$$

for $i, j = 1, 2, 3$, where G is the shear modulus, ν is the Poisson ratio, and δ_{ij} is equal to 1 if $i = j$ and is equal to 0 otherwise. The stress tensor satisfies an equilibrium equation. In the absence of body forces, the equilibrium equation is simply

$$\nabla \cdot \sigma = \mathbf{0}. \quad (2.6)$$

In summary of the linear elasticity theory of dislocations, the stress and strain tensors associated with dislocations are obtained by solving Eqs. (2.1) (or equivalently (2.2)), (2.3), (2.4), and (2.6).

Now we focus on dislocations in an isotropic infinite medium, in which the constitutive equations are given by Eq. (2.5) and there is no boundary effect.

For a screw dislocation in the $+z$ direction, i.e., $\xi = (0, 0, 1)$ and $\mathbf{b} = (0, 0, b)$, the displacement vector $\mathbf{u} = (0, 0, \frac{b}{2\pi}\theta)$, where θ is the angle in the polar coordinates of the xy plane. The strain and stress tensors are

$$\epsilon = \frac{b}{4\pi} \begin{pmatrix} 0 & 0 & -\frac{y}{x^2+y^2} \\ 0 & 0 & \frac{x}{x^2+y^2} \\ -\frac{y}{x^2+y^2} & \frac{x}{x^2+y^2} & 0 \end{pmatrix} \quad (2.7)$$

and

$$\sigma = \frac{Gb}{2\pi} \begin{pmatrix} 0 & 0 & -\frac{y}{x^2+y^2} \\ 0 & 0 & \frac{x}{x^2+y^2} \\ -\frac{y}{x^2+y^2} & \frac{x}{x^2+y^2} & 0 \end{pmatrix}. \quad (2.8)$$

Note that there is a jump of the amount \mathbf{b} in the displacement \mathbf{u} across the half plane $x > 0$ and $y = 0$, which is the cut in the definition of the screw dislocation. The value of the displacement depends on the position of the cut, i.e., the way in which the dislocation is imagined to be formed. Different choices of the cut give different values of the integration constant in the displacement. However, the strain and stress tensors do not depend on the position of the cut.

For an edge dislocation in the $+z$ direction with Burgers vector $\mathbf{b} = (b, 0, 0)$, the displacement $\mathbf{u} = (u_1, u_2, u_3)$ is

$$\begin{aligned} u_1 &= \frac{b}{2\pi} \left[\theta + \frac{xy}{2(1-\nu)(x^2+y^2)} \right], \\ u_2 &= -\frac{b}{2\pi} \left[\frac{1-2\nu}{4(1-\nu)} \log(x^2+y^2) + \frac{x^2-y^2}{4(1-\nu)(x^2+y^2)} \right], \\ u_3 &= 0. \end{aligned} \quad (2.9)$$

Again the cut is the half plane $x > 0$ and $y = 0$, and for any other cut, there is an integration constant in the displacement. The strain and stress tensors are

$$\epsilon = \frac{b}{4\pi} \begin{pmatrix} -\frac{y(x^2 - y^2)}{(1 - \nu)(x^2 + y^2)^2} - \frac{2y}{x^2 + y^2} & \frac{x(x^2 - y^2)}{(1 - \nu)(x^2 + y^2)^2} & 0 \\ \frac{x(x^2 - y^2)}{(1 - \nu)(x^2 + y^2)^2} & \frac{y(3x^2 + y^2)}{(1 - \nu)(x^2 + y^2)^2} - \frac{2y}{x^2 + y^2} & 0 \\ 0 & 0 & 0 \end{pmatrix} \quad (2.10)$$

and

$$\sigma = \frac{Gb}{2\pi(1 - \nu)} \begin{pmatrix} -\frac{y(3x^2 + y^2)}{(x^2 + y^2)^2} & \frac{x(x^2 - y^2)}{(x^2 + y^2)^2} & 0 \\ \frac{x(x^2 - y^2)}{(x^2 + y^2)^2} & \frac{y(x^2 - y^2)}{(x^2 + y^2)^2} & 0 \\ 0 & 0 & -\frac{2\nu y}{x^2 + y^2} \end{pmatrix}. \quad (2.11)$$

In the elasticity theory, the elastic energy is

$$W = \int \sum_{i,j=1,2,3} \frac{1}{2} \sigma_{ij} \epsilon_{ij} dx dy dz. \quad (2.12)$$

For a screw dislocation, the elastic energy per unit length along itself, in the cylinder $r_0 \leq r \leq R$ where r is the distance to the dislocation, is

$$W = \frac{Gb^2}{4\pi} \log \frac{R}{r_0}. \quad (2.13)$$

For an edge dislocation, the elastic energy per unit length along itself in this cylinder is

$$W = \frac{Gb^2}{4\pi(1 - \nu)} \log \frac{R}{r_0}. \quad (2.14)$$

Generally, for a straight dislocation, if the angle between the dislocation and its Burgers vector is β , the elastic energy per unit length along itself in this cylinder is

$$W = \frac{Gb^2}{4\pi} \left(\cos^2 \beta + \frac{\sin^2 \beta}{1 - \nu} \right) \log \frac{R}{r_0}. \quad (2.15)$$

We can see that the elastic energy is divergent when $r_0 \rightarrow 0$ and $R \rightarrow \infty$. The divergence at the infinity implies that the elastic energy depends on the size of the crystal. For a real crystal, R can be chosen approximately as the distance to the crystal surface, or one half of the average distance between dislocations when the crystal contains many dislocations with different signs and the long-ranged logarithm divergence is canceled out. The divergence of the elastic energy on dislocation itself ($r_0 = 0$) is due to the linear elasticity approximation, which does not apply in a small region near dislocation because

the strain is large there. This small region surrounding the dislocation is known as the core region of the dislocation, whose radius is of the order of the magnitude of Burgers vector. Inside the dislocation core region, the heavily distorted atomic structure needs to be described by atomistic models, see sections 3 and 4. However, the core energy is small compared with the elastic energy outside the core region, in other words, the main contribution to the total energy is the elastic energy outside the dislocation core region.

The strain and stress fields are also singular on the dislocation line. In the framework of the continuum theory, the singularities in the stress field and the elastic energy in the core region of the dislocation can be removed by some treatment such as simple cut-off, averaging of the results of the two nearby segments, or using smeared delta function in Eq.(2.2) instead of the exact one (which is equivalent to regarding a dislocation as a distribution of the Burgers vector inside a tube with the core radius). One method to incorporate the atomic lattice effect into the continuum theory is the Peierls-Nabarro model, which will be described in Section 4.

For a general case, the solution of the displacement is given by the Burgers formula [9]

$$\mathbf{u}(\mathbf{r}) = \frac{\mathbf{b}}{4\pi} \int_A \frac{(\mathbf{r}' - \mathbf{r}) \cdot d\mathbf{A}}{|\mathbf{r}' - \mathbf{r}|^3} - \frac{1}{4\pi} \int_C \frac{\mathbf{b} \times d\mathbf{l}'}{|\mathbf{r}' - \mathbf{r}|} + \frac{1}{8\pi(1-\nu)} \nabla \int_C \frac{\mathbf{b} \times (\mathbf{r}' - \mathbf{r}) \cdot d\mathbf{l}'}{|\mathbf{r}' - \mathbf{r}|}, \quad (2.16)$$

where C is the dislocation loop, A is a surface spanning loop C on which the jump of the displacement is \mathbf{b} , $\mathbf{r} = (x, y, z)$, and $\mathbf{r}' = (x', y', z')$. The stress tensor is given by the Peach-Koehler formula [16]

$$\begin{aligned} \sigma(\mathbf{r}) = & \frac{G}{4\pi} \int_C (\mathbf{b} \times \nabla') \frac{1}{|\mathbf{r}' - \mathbf{r}|} \otimes d\mathbf{l}' + \frac{G}{4\pi} \int_C d\mathbf{l}' \otimes (\mathbf{b} \times \nabla') \frac{1}{|\mathbf{r}' - \mathbf{r}|} \\ & - \frac{G}{4\pi(1-\nu)} \int_C \nabla' \cdot (\mathbf{b} \times d\mathbf{l}') (\nabla \otimes \nabla - \mathbf{I}\Delta) |\mathbf{r}' - \mathbf{r}|, \end{aligned} \quad (2.17)$$

where ∇' is the gradient with respect to the variables with prime. The interaction energy of two dislocation loops C_1 and C_2 is given by the Blin's formula [17]

$$\begin{aligned} W_{12} = & -\frac{G}{2\pi} \int_{C_1} \int_{C_2} \frac{(\mathbf{b}_1 \times \mathbf{b}_2) \cdot (d\mathbf{l}_1 \times d\mathbf{l}_2)}{|\mathbf{r}_1 - \mathbf{r}_2|} + \frac{G}{4\pi} \int_{C_1} \int_{C_2} \frac{(\mathbf{b}_1 \cdot d\mathbf{l}_1)(\mathbf{b}_2 \cdot d\mathbf{l}_2)}{|\mathbf{r}_1 - \mathbf{r}_2|} \\ & + \frac{G}{4\pi(1-\nu)} \int_{C_1} \int_{C_2} (\mathbf{b}_1 \times d\mathbf{l}_1) \cdot (\nabla \otimes \nabla |\mathbf{r}_1 - \mathbf{r}_2|) \cdot (\mathbf{b}_2 \times d\mathbf{l}_2). \end{aligned} \quad (2.18)$$

These formulas can be obtained using the Green's functions, see, for example, [5, 6, 14, 15]. They also have other equivalent forms. A formula under the periodic boundary conditions was obtained using the Fourier transform in [18] (see Eq.(6.4) in Section 6).

From Eq.(2.12), the elastic energy associated with a dislocation loop can be written as

$$W = \int_A \mathbf{b} \cdot \boldsymbol{\sigma} \cdot d\mathbf{A}, \quad (2.19)$$

where A is a surface spanning the dislocation loop. The force acting on the dislocation can be obtained by taking variation of this energy, which is

$$\mathbf{F} = \sigma \cdot \mathbf{b} \times \xi, \quad (2.20)$$

where ξ is the unit tangent vector of the dislocation. This equation was derived first by Peach and Koehler [16] and is referred to as the Peach-Koehler force. The stress field σ in the equation includes the applied stress field and the stress field generated by the dislocation.

As an example of the interaction between dislocations, consider two edge dislocations in the xz plane with line direction $(0, 0, 1)$ and Burgers vector $\mathbf{b} = (b, 0, 0)$, and separated by a distance r to each other. Assume that the first one is located at $x = y = 0$ and the second one is located at $x = r$ and $y = 0$. From Eq.(2.11), the stress generated by the first dislocation at the position of the second dislocation is

$$\sigma = \frac{Gb}{2\pi(1-\nu)} \begin{pmatrix} 0 & \frac{1}{r} & 0 \\ \frac{1}{r} & 0 & 0 \\ 0 & 0 & 0 \end{pmatrix}. \quad (2.21)$$

Therefore the Peach-Koehler force (Eq.(2.20)) generated by the first dislocation and acting on the second dislocation is $\frac{Gb}{2\pi(1-\nu)r}$. We can see that the force is proportional to $1/r$ and is repulsive for these two edge dislocations with the same sign. If we change the line direction of the second dislocation to $(0, 0, -1)$, which is in the opposite direction with respect to the first one, then the interaction force between them becomes attractive. The self-stress of a straight infinite dislocation does not generate a force on itself. For a curved dislocation, the leading order effect of the self-stress is the line tension (direction dependent), which generates a force proportional to its curvature and perpendicular to itself in the direction to shorten its length.

Dislocation migration can, at low velocities, be thought of as purely dissipative, such that the local dislocation velocity can be written as

$$\mathbf{v} = \mathbf{M} \cdot \mathbf{F}, \quad (2.22)$$

where \mathbf{M} is the mobility tensor. Recall that glide is the motion of a dislocation in its slip plane (the plane containing its line direction and Burgers vector), and climb is the motion of a dislocation in the direction perpendicular to the slip plane. Since climb is much more difficult than glide at low temperatures, the climb mobility is much smaller than that of the glide. More generally, the stress dependence of the dislocation velocity is fitted by the power law $v = v_0(\sigma/\sigma_0)^n$ or $v = v_0 \exp(-\sigma_0/\sigma)$, where v is a component of the dislocation velocity, σ is the appropriate component of stress to generate v , and v_0 , σ_0 and n are constants, see e.g., [5, 6, 12, 14, 19–21].

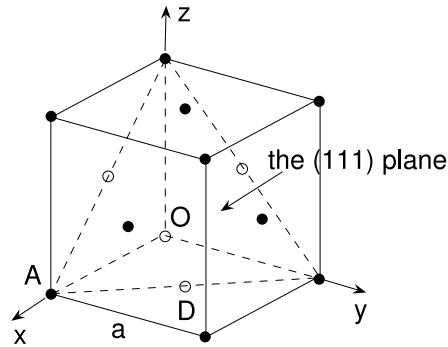


Figure 8: An FCC lattice.

3 Dislocations in crystals: atomistic models

We have seen in the previous section that the continuum dislocation theory does not apply in the core region of a dislocation, which is at the length scale of several lattice constants surrounding the dislocation. The atomic arrangement and the stress and strain fields of dislocations in the core region depend strongly on the crystal structures. Many properties of dislocations, such as the dislocation slip system (the possible Burgers vectors and slip planes), the mobility of dislocations, and the reaction between dislocations, are determined by the crystal structures and the dislocation core properties, and play important roles in the plastic deformation of crystals.

Real crystals have structures more complicated than the simple cubic lattice, such as the face-centred cubic (FCC) structure, the body-centred cubic (BCC) structure, the diamond cubic structure, and the hexagonal close-packed (HCP) structure, etc. In this section, we introduce some models and properties of dislocations in crystals with the FCC structure. More about the models and properties of dislocations in particular crystal structures can be found, for example, in [5–7, 12, 13, 22–29].

Fig. 8 shows the FCC crystal structure. The unit cell of this structure is a cube, with an atom situated on each corner and each face center. The lattice constant a is the length of each edge of the cube. The crystal lattice is formed by repeating this unit cell periodically in the whole space. Many common metals such as copper (Cu) and aluminum (Al) have this FCC crystal structure. Using Miller indices, an atomic plane in the crystal lattice can be described by (hkl) , where the direction (h, k, l) in the atomic coordinate system is in the normal direction of the plane, and h , k and l are three integers (smallest among all choices). If the intercept of a plane on some axis, say on the x axis, is negative, then the indices of this plane are $(\bar{h}kl)$, where h , k and l are positive integers. As an example, the (111) plane is shown in Fig. 8. The notation $\{hkl\}$ is used to represent all the planes of the same crystallography type as the (hkl) plane. For example, $\{111\} = \{(111), (\bar{1}11), (1\bar{1}1), (11\bar{1})\}$. A direction in the crystal lattice is described by $[hkl]$, which means the three components of the direction in the atomic coordinate system are ha , ka , la , respectively. For example, in Fig. 8, the vector OA

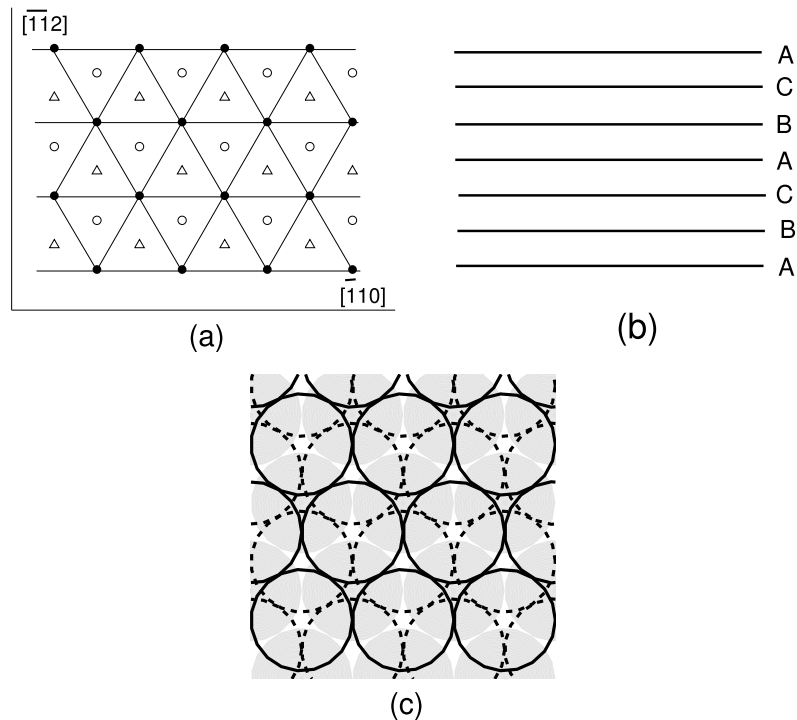


Figure 9: The atomic arrangement on (111) planes and the stacking in $[111]$ direction. (a) The atomic arrangement on (111) planes. The dots show the atomic sites on a (111) planes. The triangles show the atomic sites on the first layer above projected onto this plane. The circles show the atomic sites on the second layer above projected onto this plane. The projected positions of the atomic sites on the third layer above coincide with those on the plane. (b) The stacking sequence in $[111]$ direction, which is pointing upward. (c) The atomic arrangement on (111) planes using the hard ball model. The stacking of the balls is layer by layer in the $[111]$ direction, which is pointing out of the paper. The filled circles, dashed circles and circles show the positions of the atoms on one layer (say, layer A), the first layer above (layer B), and the second layer above (layer C), respectively. The positions of the atoms on the third layer above projected on the paper coincide with those on the layer A.

is $[100]$ and the vector AD is $\frac{1}{2}[\bar{1}10]$. The notation $\langle hkl \rangle$ is used to represent all the directions of the same crystallography type as the $[hkl]$ direction. For example, $\langle 110 \rangle = \{[110], [\bar{1}10], [1\bar{1}0], [\bar{1}\bar{1}0], [101], [\bar{1}01], [10\bar{1}], [\bar{1}0\bar{1}], [011], [0\bar{1}1], [01\bar{1}], [0\bar{1}\bar{1}]\}$. For the dislocations in an FCC crystal, the most energetically favored Burgers vectors are the smallest lattice vectors $\frac{1}{2}\langle 110 \rangle$, and the most energetically favored slip planes are $\{111\}$ planes, which are the most close-packed planes containing the Burgers vectors $\frac{1}{2}\langle 110 \rangle$.

The atomic arrangement on a (111) plane is shown in Fig. 9(a). The arrangement has a triangular lattice structure. The distance between two adjacent (111) planes is $a/\sqrt{3}$. The projected positions of the lattice sites of the atoms on the first layer and second layer above the plane are also shown in Fig. 9(a). The projected positions of the atomic sites on the third layer above the plane coincide with those on the plane. So in $[111]$ direction, the atomic arrangement follows the stacking sequence $\cdots ABCABC \cdots$, as shown in Fig. 9(b). This stacking can be imaged as the stacking of hard spherical balls, see Fig. 9(c). These

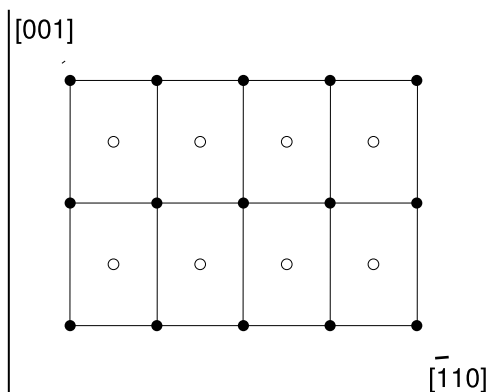


Figure 10: The atomic arrangement on (110) planes. Dots show the atomic sites on a (110) plane. Circles show the projected positions of the atomic sites on the first layer above this plane. The projected positions of the atomic sites on the second layer above the plane coincide with those on the plane.

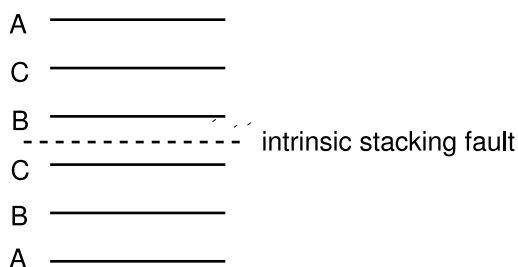


Figure 11: An intrinsic stacking fault between layers C and B. The layer A between these layers C and B in the stacking sequence of a perfect crystal is missing.

$\{111\}$ planes are the slip planes of the perfect dislocations, whose Burgers vectors are $\frac{1}{2} \langle 110 \rangle$ vectors that connect two adjacent atoms in the slip plane.

The atomic arrangement on a (110) plane and on the first layer above it is shown in Fig. 10. The projected positions of the atomic sites on the second layer above the plane coincide with those on the plane. So in $[110]$ direction, the atomic arrangement follows the stacking sequence $\cdots ABABAB \cdots$.

If in the stacking sequence in the $[111]$ direction $\cdots ABCABCA \cdots$, one layer, say the A layer in the middle, is missing, then the stacking sequence becomes $\cdots ABCBCA \cdots$, and there is a stacking fault between the layers C and B in the middle, as shown in Fig. 11. Now consider the layer C right below the stacking fault. The layer below it (which is a B layer) is the same as that in the perfect lattice. The layer above it (which is also a B layer) is different than that in a perfect lattice (which is an A layer), but the relative positions of the atoms on the two layers are the same, see Fig. 9(a). The difference of the relative positions of atoms starts from the second layer above this layer C. So the stacking fault does not increase the total energy very much. The stacking fault energy γ is defined as the energy difference between the lattices with and without a stacking fault, divided by the area of the stacking fault. The stacking fault described above is called intrinsic

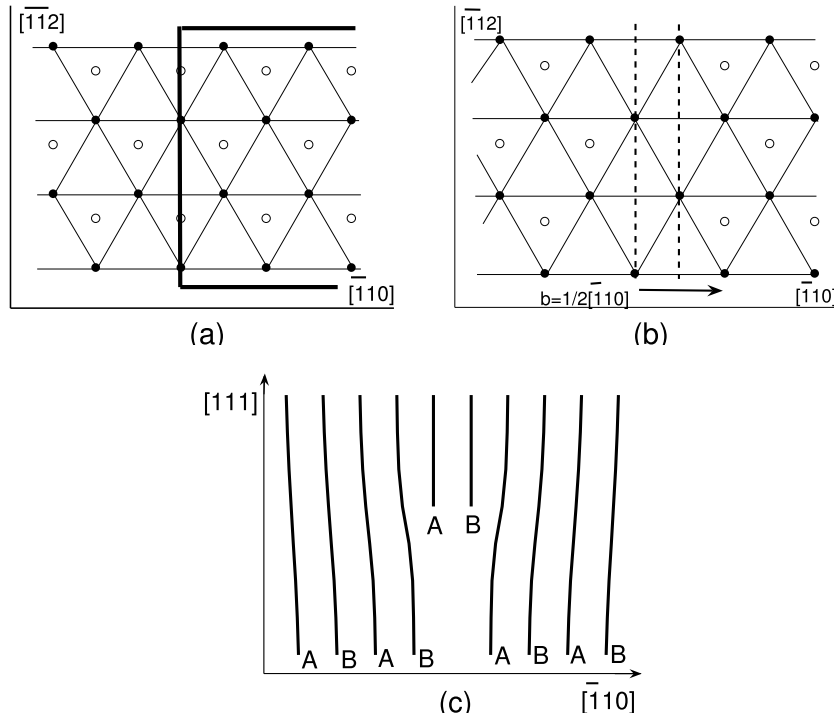


Figure 12: A perfect edge dislocation in the FCC lattice. (a) Atomic sites on a (111) plane (dots, layer A) and the projected positions of the atomic sites on the first layer below (circles, layer C). A half plane cut will be made between these two layers (as shown on the right of the image). (b) The atomic sites of these two layers after the cut and a relative shift of the amount of the Burgers vector $\mathbf{b} = \frac{1}{2}[\bar{1}10]$. Two rows of atoms on the layer below the cutting plane are missing (same for all layers below the cut). The edge dislocation is formed after elastic deformation from this configuration. (c) Stacking sequence of the edge dislocation in $[\bar{1}10]$ direction.

stacking fault. There are other stacking faults such as the extrinsic stacking fault, which is formed by adding one layer in the stacking sequence of a perfect lattice.

Now consider an edge dislocation in an FCC crystal with Burgers vector $\mathbf{b} = \frac{1}{2}[\bar{1}10]$ and in the direction of $[11\bar{2}]$ in the slip plane (111). It can be imagined as being formed by making a half-plane cut between two layers in the $[111]$ direction, say layers C and A, in the stacking sequence $\dots ABCABC \dots$ in a perfect lattice, and then shifting the atoms above and below the cut relatively by the amount of the Burgers vector \mathbf{b} . Fig. 12(a) shows the atomic sites of these two layers C and A in a perfect lattice and the position of the cut. Fig. 12(b) shows the atomic sites of these two layers after the cut and shift. To explain more clearly, the positions of atoms in Fig. 12(b) are still plotted in the perfect triangular lattice sites. For an edge dislocation, the lattice near the dislocation line (the edge of the cut) is heavily distorted. This edge dislocation can also be imagined as being formed by adding two half planes of atoms on and above the layer A or by removing two half planes of atoms on and below the layer C, as shown in Fig. 12(c).

Now imagine an edge dislocation formed by adding two half planes of atoms, as shown

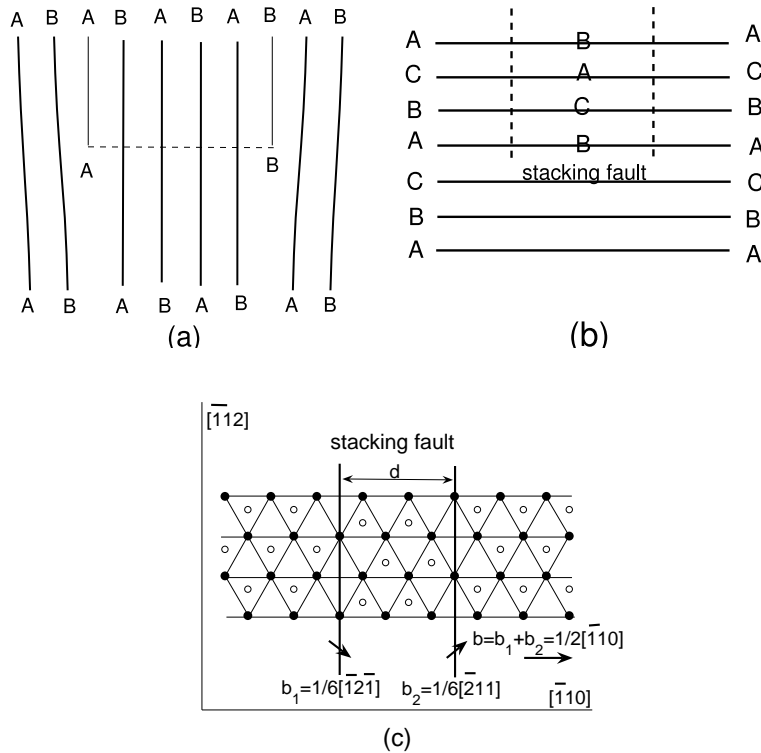


Figure 13: Extended edge dislocation consisting of Shockley partials. (a) Stacking sequence in $[\bar{1}10]$ direction (pointing to the right) for an edge dislocation. The two extra half planes (two partials) are separated. (b) Stacking sequence in $[111]$ direction (pointing upward) for the edge dislocation. There is a stacking fault between two partials on the (111) plane containing the extended edge dislocation. (c) The atomic arrangement on the layers right above and below the slip plane of the extended edge dislocation. The dots and circles show the atomic sites on the layers above and below the slip plane, respectively. To explain more clearly, the positions of atoms are still plotted in the perfect triangular lattice sites. The extended dislocation is formed after elastic deformation from this configuration.

in Fig. 12(c). The two layers may be separated, as shown in Fig. 13(a). This corresponds to the dissociation of the edge dislocation with Burgers vector $\mathbf{b} = \frac{1}{2}[\bar{1}10]$ into two dislocations with Burgers vectors $\mathbf{b}_1 = \frac{1}{6}[\bar{1}2\bar{1}]$ and $\mathbf{b}_2 = \frac{1}{6}[\bar{2}11]$, respectively. Since $|\mathbf{b}| = a/\sqrt{2}$ and $|\mathbf{b}_1| = |\mathbf{b}_2| = a/\sqrt{6}$, from the Frank's rule described in Section 1, this dissociation is energetically favored. The original dislocation is a perfect dislocation, whose Burgers vector is a lattice vector. The dissociation results in two dislocations, whose Burgers vectors are not lattice vectors. These two dislocations are called partial dislocations. On the other hand, when the dissociation happens, the atoms above and below the slip plane between the two partial dislocations are not in their equilibrium positions. They are in the positions of a stacking fault, as shown in Fig. 13 (b) and (c). This increases the total energy by the amount of the stacking fault energy γ multiplied by the area of the stacking fault. The energy minimum state is reached when the two partials are separated by a distance d . The value of d can be estimated from the continuum dislocation theory. Using

the Peach-Koehler force introduced in the previous section, it can be shown that

$$d \approx \frac{(2 + \nu)Ga^2}{48\pi(1 - \nu)\gamma}. \quad (3.1)$$

Therefore the stable structure of this edge dislocation consists of two partials separated by a distance d . This structure is called extended dislocation, as shown in Fig. 13(c). When a perfect dislocation with Burgers vector $\frac{1}{2} \langle 110 \rangle$ (not necessarily an edge dislocation) is dissociated into two partials with Burgers vectors $\frac{1}{6} \langle 112 \rangle$, the partials are known as the Shockley partials [30]. Note that the Burgers vectors of the two Shockley partials are all in the slip plane of the original perfect dislocation, so this plane is also their slip plane and they can move in it by glide. For example, in copper, the distance d between the two Shockley partials of an edge dislocation is about $10a$, where a is the lattice constant of copper. There are also other types of partials such as the Frank partials [31] in the FCC crystals.

Usually, atomistic methods such as the empirical interatomic potential simulations or first principles calculations are used to study the core related properties [5, 7, 22, 24, 25, 27–29, 32–42]. For example, in [38], the lattice resistance to dislocation motion in aluminum under pressure was examined by employing the embedded atom (EAM) potential [43] for aluminum [44], which is

$$E = \sum_i F(\rho_i) + \frac{1}{2} \sum_{i \neq j} V(R_{ij}), \quad (3.2)$$

where i and j are the indices for the atoms, R_{ij} is the distance between atoms i and j , V is the two-body potential, F is the embedding function, and ρ_i is the electronic density felt by atom i , which can be written as

$$\rho_i = \sum_{j \neq i} \rho(R_{ij}) \quad (3.3)$$

where ρ is the electron density function. The functions V , F and ρ are fitted functions from the quantum mechanical data [44]. The force acting on the i -th atom \mathbf{f}_i can be calculated from the energy Eq.(3.2):

$$\mathbf{f}_i = - \sum_{j \neq i} [F'(\rho_i)\rho'(R_{ji}) + F'(\rho_j)\rho'(R_{ji}) + V'(R_{ji})] \mathbf{R}_{ji}/R_{ji}, \quad (3.4)$$

where \mathbf{R}_{ji} is the vector between the j -th atom and the i -th atom and pointing to the latter. The equilibrium atom positions can be obtained by minimizing the potential energy using the conjugate gradient relaxation technique [45].

Sometimes, the continuum theory can also be used to study the dislocation core structure with some information (such as the stacking fault energy γ) provided by the atomistic models. The estimate for the core width given in Eq.(3.1) is a simple example. Some recent results using this method can be found, for example, in [46, 47].

Another method to study the dislocation core structure is the Peierls-Nabarro model [5, 48, 49], which will be discussed in the next section.

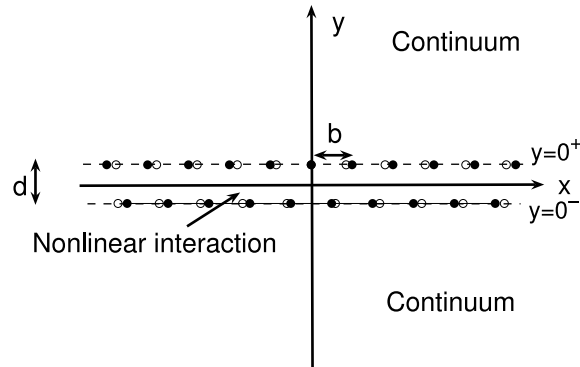


Figure 14: Peierls-Nabarro model for an edge dislocation. Two half spaces are treated as elastic continua and the interaction between them is nonlinear. The dots show the positions of the atoms above and below the slip plane after two half spaces are placed together with an initial disregistry Eq.(4.1). The circles show the positions of the atoms above and below the slip plane in the edge dislocation after minimization of the total energy (for simplicity, the vertical displacement is not shown).

4 The Peierls-Nabarro model

As mentioned in the previous sections, the energy associated with the dislocations is stored in the whole medium. At the length scale of several lattice constants away from the dislocations, i.e., outside the core region of the dislocations, the strain and stress fields are described well by the continuum dislocation theory. Within the core region of the dislocations, the continuum theory does not apply, and atomistic models are used to describe the details of the dislocation cores. These atomistic simulations are time consuming and cannot be used to study the dislocations at the length scales much larger than the core size. The Peierls-Nabarro model [48, 49] incorporates the atomic effect into the continuum model, therefore provide an alternative way to understand the core-related properties, such as the core structure and mobility of the dislocations, in the continuum framework.

In the framework of the Peierls-Nabarro models, the solid is divided by the slip plane of the dislocation into two half-space linear elastic continua, which have a misfit relative to each other and are connected by a nonlinear potential force. The dislocation is the equilibrium state after the minimization of the total energy, which includes the elastic energy in the two half-space continua, and the misfit energy due to the nonlinear atomic interaction across the slip plane. As an example, we describe the Peierls-Nabarro model for an edge dislocation below. More can be found, for example, in [5–7, 12–14, 24, 26, 48–50].

Assume that the lattice is simple cubic, the edge dislocation is located along the z axis and its line direction is in the $+z$ direction, the Burgers vector is in the $+x$ direction: $\mathbf{b} = (b, 0, 0)$, and therefore the slip plane of this edge dislocation is the xz plane. The cross section of this edge dislocation is shown in Fig. 14. The lattice spacing in the x direction is the length of the Burgers vector b , the lattice spacing in the y direction, which is perpendicular to the slip plane, is d . To form the edge dislocation, imagine that two

half spaces of atoms $y > 0$ and $y < 0$ are placed together along the plane $y = 0$ with a disregistry of the top half with respect to the bottom one

$$\phi(x) = \begin{cases} b/2, & x > 0 \\ -b/2, & x < 0, \end{cases} \quad (4.1)$$

as shown in Fig. 14. This can be understood as that there is an extra half plane of atoms at $x = 0$ and $y > 0$ inserted into the upper half space of a perfect lattice, and when $x > 0$, the atoms on the top half are shifted relative to the bottom half atoms by the amount of $b/2$ in the $+x$ direction; while when $x < 0$, the shift is $b/2$ in the $-x$ direction. Both the half spaces $y > 0$ and $y < 0$ are considered as linear elastic continuums, connected by some nonlinear potential force along the plane $y = 0$. The edge dislocation is formed through the minimization of the total energy including the elastic energy in the two half-space continuums $y > 0$ and $y < 0$, and the misfit energy due to the nonlinear atomic interaction across the slip plane $y = 0$, by the elastic deformation in the two half spaces. Based on the symmetry of the initial configuration, it is assumed that during the elastic deformation, on the interface $y = 0$ we have

$$\begin{cases} u_1(x, 0^+) = -u_1(x, 0^-), & u_1(+\infty, 0^+) = -b/4, & u_1(-\infty, 0^+) = b/4, \\ u_2(x, 0^+) = u_2(x, 0^-), \end{cases} \quad (4.2)$$

where u_1 and u_2 are the components of the displacement vector in the x and y directions, respectively. After the edge dislocation is formed, the disregistry of the top half with respect to the bottom one becomes

$$\phi(x) = \begin{cases} 2u(x) + b/2, & x > 0 \\ 2u(x) - b/2, & x < 0, \end{cases} \quad (4.3)$$

where $u(x) = u_1(x, 0^+) = -u_1(x, 0^-)$.

From the continuum dislocation theory (Eq.(2.11)), the force in x direction per unit area in the interface $y = 0$ plane is the shear stress

$$\sigma_{12}(x, 0) = \frac{G}{2\pi(1-\nu)} \int_{-\infty}^{+\infty} \frac{-2u'(x')}{x-x'} dx'. \quad (4.4)$$

Here we have used the fact that the distribution of the Burgers vector on the x axis is $\rho(x) = -2u'(x)$. This can be understood as follows. If we draw a small circular loop in the counterclockwise direction with its center located on $(x, 0)$ and intersecting the x -axis at $(x - \frac{1}{2}\Delta x, 0)$ and $(x + \frac{1}{2}\Delta x, 0)$, where $\Delta x > 0$, then by the definition (Eq.(2.1)), the Burgers vector contained inside this loop is

$$\begin{aligned} & \left[u_1 \left(x - \frac{1}{2}\Delta x, 0^+ \right) - u_1 \left(x + \frac{1}{2}\Delta x, 0^+ \right) \right] + \left[u_1 \left(x + \frac{1}{2}\Delta x, 0^- \right) - u_1 \left(x - \frac{1}{2}\Delta x, 0^- \right) \right] \\ &= 2u \left(x - \frac{1}{2}\Delta x \right) - 2u \left(x + \frac{1}{2}\Delta x \right) \\ &\approx -2u'(x)\Delta x. \end{aligned} \quad (4.5)$$

If we use the strict definition of the Burgers vector Eq.(2.1) for this edge dislocation, the distribution of the Burgers vector should be the delta-function at $x = 0$, i.e., $-2u'(x) = \delta(x)$. In the Peierls-Nabarro model, the distribution of the Burgers vector is no longer a strict delta-function, but is determined by the nonlinear interplanar force across the slip plane, as will show below. Note that the stress formula Eq.(4.4) can also be obtained by solving the elasticity problems in the two half spaces $y > 0$ and $y < 0$, respectively, using the boundary conditions Eq.(4.2).

The interplanar misfit energy due to the disregistry $\phi(x)$ between the the two half spaces $y > 0$ and $y < 0$ is

$$W_{\text{misfit}} = \int_{-\infty}^{+\infty} E(\phi(x))dx, \quad (4.6)$$

where the energy density $E(\phi)$ is approximated by [8]

$$E(\phi) = \frac{Gb^2}{4\pi^2d} \left(1 - \cos \frac{2\pi\phi}{b} \right). \quad (4.7)$$

The interplanar force per unit area (the restoring stress) is obtained by taking variation of this energy, which is in x direction and its value per unit area is

$$\tau = \frac{Gb}{2\pi d} \sin \frac{2\pi\phi}{b}. \quad (4.8)$$

This simple sinusoidal approximation for the misfit energy guarantees that the energy attains its minimum for a perfect lattice $\phi = nb$, n integer, and when ϕ is small, the force reduces to the Hooke's law in the linear elasticity: $\tau = G\phi/d$ (recall that d is the interplanar distance). Using Eq.(4.3), the interplanar restoring force per unit area for the edge dislocation can be written as

$$\tau = -\frac{Gb}{2\pi d} \sin \frac{4\pi u}{b}. \quad (4.9)$$

Since $\phi(x)$ is the disregistry of the top half with respect to the bottom half, this force is acting on the atoms right below the $y = 0$ plane.

After energy minimization, the forces acting on the interface $y = 0$ from the elastic energy and misfit energy should be balanced. Combining Eqs. (4.4) and (4.9), one has the equation

$$\frac{G}{2\pi(1-\nu)} \int_{-\infty}^{+\infty} \frac{2u'(x')}{x-x'} dx' = \frac{Gb}{2\pi d} \sin \frac{4\pi u}{b}. \quad (4.10)$$

This equation has an analytic solution, which is

$$u(x) = -\frac{b}{2\pi} \tan^{-1} \frac{x}{\zeta}, \quad (4.11)$$

where

$$\zeta = \frac{d}{2(1-\nu)}. \quad (4.12)$$

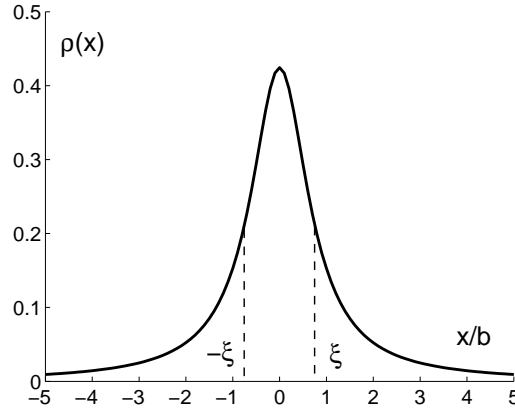


Figure 15: Distribution of the Burgers vector of an edge dislocation. Here $d = b$, $\nu = 1/3$, and $2\zeta = d/(1 - \nu)$ is the width of the dislocation core.

The distribution of the Burgers vector is

$$\rho(x) = -2u'(x) = \frac{b}{\pi} \frac{\zeta}{x^2 + \zeta^2}, \quad (4.13)$$

as shown in Fig. 15. The width of the dislocation core is defined as

$$2\zeta = \frac{d}{1 - \nu}, \quad (4.14)$$

which is of the order of the Burgers vector b .

As we can see, in the Peierls-Nabarro model, a smeared delta-function $\rho(x)$ is determined from the atomistic interaction between the two atomic layers above and below the slip plane. This smeared delta-function represents the distribution of the Burgers vector in the slip plane. Using this core model, the lattice effect is included in the continuum model, and the displacement vector, the strain and stress fields, and the elastic energy are no longer singular. The displacement vector $\mathbf{u} = (u_1, u_2, u_3)$ is

$$\begin{aligned} u_1(x, y) &= \frac{b}{2\pi} \left[-\tan^{-1} \frac{x}{y \pm \zeta} + \frac{xy}{2(1 - \nu)(x^2 + (y \pm \zeta)^2)} \right] \\ u_2(x, y) &= -\frac{b}{2\pi} \left[\frac{1 - 2\nu}{4(1 - \nu)} \log(x^2 + (y \pm \zeta)^2) + \frac{x^2 - y^2 + \zeta^2}{4(1 - \nu)(x^2 + (y \pm \zeta)^2)} \right] \\ u_3(x, y) &= 0, \end{aligned} \quad (4.15)$$

and the strain and stress fields are

$$\epsilon = \frac{b}{4\pi} \begin{pmatrix} -\frac{2(y \pm \zeta)}{x^2 + (y \pm \zeta)^2} - \frac{y[x^2 - (y \pm \zeta)^2]}{(1 - \nu)[x^2 + (y \pm \zeta)^2]^2} & \frac{x}{(1 - \nu)[x^2 + (y \pm \zeta)^2]} - \frac{2xy(y \pm \zeta)}{(1 - \nu)[x^2 + (y \pm \zeta)^2]^2} & 0 \\ \frac{x}{(1 - \nu)[x^2 + (y \pm \zeta)^2]} - \frac{2xy(y \pm \zeta)}{(1 - \nu)[x^2 + (y \pm \zeta)^2]^2} & \frac{2\nu y \pm (2\nu - 1)\zeta}{(1 - \nu)[x^2 + (y \pm \zeta)^2]} + \frac{(x^2 - y^2 + \zeta^2)(y \pm \zeta)}{(1 - \nu)[x^2 + (y \pm \zeta)^2]^2} & 0 \\ 0 & 0 & 0 \end{pmatrix} \quad (4.16)$$

and

$$\sigma = \frac{Gb}{2\pi(1-\nu)} \begin{pmatrix} -\frac{3y\pm 2\zeta}{x^2+(y\pm\zeta)^2} + \frac{2y(y\pm\zeta)^2}{[x^2+(y\pm\zeta)^2]^2} & \frac{x}{x^2+(y\pm\zeta)^2} - \frac{2xy(y\pm\zeta)}{[x^2+(y\pm\zeta)^2]^2} & 0 \\ \frac{x}{x^2+(y\pm\zeta)^2} - \frac{2xy(y\pm\zeta)}{[x^2+(y\pm\zeta)^2]^2} & -\frac{y}{x^2+(y\pm\zeta)^2} + \frac{2x^2y}{[x^2+(y\pm\zeta)^2]^2} & 0 \\ 0 & 0 & -\frac{2\nu(y\pm\zeta)}{x^2+(y\pm\zeta)^2} \end{pmatrix}, \quad (4.17)$$

where the $+\zeta$ applies for $y > 0$ and $-\zeta$ applies for $y < 0$. The elastic energy per unit length along the edge dislocation is

$$W_{\text{elastic}} = \frac{Gb^2}{4\pi(1-\nu)} \log \frac{R}{2\zeta}, \quad (4.18)$$

where R is the outer cut-off distance. Besides, the misfit energy per unit length along the edge dislocation, coming from the nonlinear interaction between the two atomic layers above and below the slip plane (Eq.(4.6)), is

$$W_{\text{misfit}} = \frac{Gb^2}{4\pi(1-\nu)}. \quad (4.19)$$

Therefore the total energy of this edge dislocation is

$$W_{\text{total}} = W_{\text{elastic}} + W_{\text{misfit}} = \frac{Gb^2}{4\pi(1-\nu)} \left(\log \frac{R}{2\zeta} + 1 \right). \quad (4.20)$$

In the above calculations, the total energy does not depend on the position of the center of the dislocation. However, due to the lattice effect, the total energy varies as the center of the profile of the dislocation is located at different positions relative to the lattice sites, which generates an energy barrier when the dislocation glides on its slip plane. This energy barrier can be estimated using the Peierls-Nabarro model by summing the misfit energy over discrete lattice sites instead of the integral in Eq.(4.6), i.e.,

$$W_{\text{misfit}} = \sum_{m=-\infty}^{+\infty} \frac{1}{2} \left[E(\phi(mb - x_c)) + E\left(\phi\left(mb + \frac{b}{2} - x_c\right)\right) \right], \quad (4.21)$$

where x_c is the center of the dislocation profile,

$$E(\phi) = \frac{Gb^2}{4\pi^2 d} \left(1 - \cos \frac{2\pi\phi}{b} \right) = \frac{Gb^2}{4\pi^2 d} \left(1 + \cos \frac{4\pi u}{b} \right), \quad (4.22)$$

and $u(x)$ is the solution when the dislocation center is at the origin, given by Eq.(4.11). This discrete summation of the energy is the average of the misfit energy of the atoms on the layers right above (the first term in the summation) and below (the second term in the summation) the slip plane.

The discrete summation in the misfit energy (4.21) can be calculated analytically [51]:

$$W_{\text{misfit}} = \sum_{n=-\infty}^{+\infty} \frac{Gb^3\zeta^2}{4\pi^2d} \cdot \frac{1}{(nb/2 - x_c)^2 + \zeta^2} = \frac{Gb^2\zeta}{2\pi d} \cdot \frac{\sinh \frac{4\pi\zeta}{b}}{\cosh \frac{4\pi\zeta}{b} - \cos \frac{4\pi x_c}{b}}. \quad (4.23)$$

When ζ is much greater than b ,

$$W_{\text{misfit}} \approx \frac{Gb^2}{4\pi(1-\nu)} \left(1 + 2e^{-\frac{4\pi\zeta}{b}} \cos \frac{4\pi x_c}{b} \right). \quad (4.24)$$

When x_c varies, the difference between the maximum and minimum of the misfit energy is

$$W_p = \frac{Gb^2}{\pi(1-\nu)} e^{-\frac{4\pi\zeta}{b}}, \quad (4.25)$$

which is the energy barrier for the glide of the dislocation and is known as the Peierls energy. The stress required for the dislocation to overcome this energy barrier is (using Eq.(2.20))

$$\sigma_p = \max \left\{ \frac{1}{b} \frac{\partial W_{\text{misfit}}}{\partial x_c} \right\} = \frac{2G}{1-\nu} e^{-\frac{4\pi\zeta}{b}}, \quad (4.26)$$

which is known as the Peierls stress. For an FCC crystal, $b = a/\sqrt{2}$, $d = a/\sqrt{3}$, where a is the lattice constant. If we choose $\nu = 1/3$, the Peierls stress is $\sigma_p = 1.36 \times 10^{-3}G$. This is much less than the critical stress to shear a perfect crystal, which is about $0.1G$ (The maximum value in Eq.(4.8)) [8]. Other qualitative observations can also be made. For example, the Peierls stress decreases as the interplanar distance d increases, therefore the dislocation is easy to move in those planes with the largest interplanar distance, i.e., the most close-packed planes, which are the slip planes of the dislocation.

The Peierls-Nabarro model is an over-simplified model. Lots of efforts have been made to improve it by incorporating more detailed atomic structures and properties [22, 52-84]. Some of these improvements are reviewed below.

One important improvement over the classic Peierls-Nabarro model is the concept of the generalized stacking fault energy (the γ surface) introduced by Vitek [22, 61, 85]. Considering a perfect crystal cut along a plane and then reconnected after a shift in a direction \mathbf{f} in the cutting plane, the generalized stacking fault energy $\gamma(\mathbf{f})$ is defined as the energy increment per unit area after the reconnection [85]. The interplanar restoring stress associated with the generalized stacking fault energy is

$$\mathbf{F}(\mathbf{f}) = -\nabla(\gamma(\mathbf{f})). \quad (4.27)$$

The classic Peierls-Nabarro is improved by replacing the Frenkel sinusoidal restoring stress Eq.(4.8) by this restoring stress [22, 61, 62], which is more accurate and applies to a misfit with any direction in the slip plane. At first the generalized stacking fault energy was calculated using the empirical potentials [22, 61, 62, 85]; now it can be obtained more

accurately using the first principles calculations [64, 66, 69, 70, 72, 73, 80]. The Peierls-Nabarro framework with the restoring force obtained from the atomistic models provides an alternative way to study the core-related properties of the dislocations such as the core structure or the mobility of the dislocations [22, 61, 62, 64, 66, 67, 69–73, 75, 76, 78, 80, 83, 84].

Another method to extend the one-dimensional Frenkel sinusoidal misfit energy to two dimensions is to use the symmetry of crystal lattices. This method was used by Leibfried and Dietze [55] to obtain the misfit energy for any two-dimensional misfit in the slip plane by approximating the summation of the misfit energy on discrete lattice sites by the Fourier expansion, before the concept of the generalized stacking fault energy was proposed. They studied the dislocation core structure by minimizing the total energy for prescribed core shapes of the arc-tangent type suggested by the analytical solution of the classic Peierls-Nabarro model Eq.(4.11). Combining these two methods, Schoeck [67] fitted the generalized stacking energy obtained from the atomistic simulations, by using sinusoidal functions based on the symmetry of crystal lattices, and applied this method to study the dislocation properties in some metals and alloys. The generalized stacking fault energy he obtained for aluminum (FCC lattice) is approximated by

$$\begin{aligned}
 \gamma(x, z) = & c_0 \\
 & + c_1[\cos 2pz + \cos(pz + qx) + \cos(pz - qx)] \\
 & + c_2[\cos 2qx + \cos(3pz + qx) + \cos(3pz - qx)] \\
 & + c_3[\cos 4pz + \cos(2pz + 2qx) + \cos(-2pz + 2qx)] \\
 & + c_4[\cos(pz + 3qx) + \cos(-pz + 3qx) + \cos(4pz + 2qx) \\
 & \quad + \cos(-4pz + 2qx) + \cos(5pz + qx) + \cos(5pz - qx)] \\
 & + a_1[\sin 2pz - \sin(pz + qx) + \sin(-pz + qx)] \\
 & + a_3[\sin 4pz - \sin(2pz + 2qx) + \sin(-2pz + 2qx)], \tag{4.28}
 \end{aligned}$$

where $p = 2\pi/(\sqrt{3}b)$, $q = 2\pi/b$, constants $c_1, c_2, c_3, c_4, a_1, a_3$ are fitted from the first principles simulation data [73]. Here the slip plane is the xz plane and the Burgers vector is in $+x$ direction.

Modifications have also been made to use the anisotropic elasticity instead of the isotropic one for the elastic energy in the two half-space elastic continuums [52, 58, 67]. Eshelby [52] considered the edge dislocations in anisotropic materials. Seeger and Schoeck [58] studied the separation of two Shockley partials and their recombination energy for dissociated edge and screw dislocations in Cu and Al, using the prescribed core shapes of the arc-tangent type proposed in [55], and accounting for the elastic anisotropy. For a general straight dislocation, under the anisotropic elasticity theory of dislocations [5, 86–88], the elastic energy in the two half-space continuums in an anisotropic material can be written as (Schoeck [67])

$$W_{\text{elastic}} = \int_{-\infty}^{\infty} \int_{-\infty}^{\infty} \frac{1}{4\pi} \frac{d\mathbf{u}(s)}{ds} \frac{\mathbf{H}}{s-x} \mathbf{u}(x) ds dx, \tag{4.29}$$

where \mathbf{u} is the displacement vector, \mathbf{H} is the Stroh tensor of the prelogarithmic energy factors. In an isotropic material, the Stroh tensor is

$$\mathbf{H} = G \begin{pmatrix} \frac{1}{1-\nu} & 0 & 0 \\ 0 & \frac{1}{1-\nu} & 0 \\ 0 & 0 & 1 \end{pmatrix}. \quad (4.30)$$

For a straight dislocation in an anisotropic material, numerical calculation is needed to obtain the Stroh tensor except for some special cases.

In the classic Peierls-Nabarro model, the dislocation core structure is obtained by minimizing the total energy including the elastic energy and the misfit energy; while the Peierls energy and Peierls stress are not directly obtained from energy minimization, instead, they are calculated by a summation of the misfit energy over discrete lattice sites after the continuum distribution of the Burgers vector is obtained. To remove this inconsistency, Bulatov and Kaxiras [72] proposed a semidiscrete framework, in which the elastic energy is also expressed as a discrete summation on lattice sites so that the Peierls energy and Peierls stress can be obtained by minimizing the total energy written in discrete summation. In their new framework, the elastic energy is discretized from the continuous expression by assuming that the strain, stress, and the distribution of the Burgers vector are piecewise constant near each nodal point representing the lattice site of atoms on the slip plane. The Peierls energy is identified as the difference between the maximum and minimum of the total energy when the center of the dislocation profile varies in the slip direction. When external stress is applied, the dislocation profile is solved by minimizing the total energy including the elastic energy, the misfit energy, and the interaction energy between the displacement and the applied stress. The Peierls stress is defined as the critical value of the applied stress, at which no stable dislocation profile can be found by the energy minimization. For the misfit energy, they use generalized stacking fault energy obtained from the first principle calculations, in which the opening in the direction perpendicular to the slip plane is also considered. The total energy in their model is

$$W_{\text{total}} = W_{\text{elastic}} + W_{\text{misfit}} + W_{\text{stress}} + Kb^2 \log L, \quad (4.31)$$

where

$$W_{\text{elastic}} = \sum_{i,j} \frac{1}{2} \chi_{ij} [K_e (\rho_i^{(1)} \rho_j^{(1)} + \rho_i^{(2)} \rho_j^{(2)}) + K_s \rho_i^{(3)} \rho_j^{(3)}], \quad (4.32)$$

$$W_{\text{misfit}} = \sum_i \Delta x \gamma_3(\mathbf{f}_i), \quad (4.33)$$

$$W_{\text{stress}} = - \sum_{i,l} \frac{x_i^2 - x_{i-1}^2}{2} \rho_i^{(l)} \tau_i^{(l)}, \quad (4.34)$$

$$K = \frac{G}{2\pi} \left(\frac{\sin^2 \beta}{1-\nu} + \cos^2 \beta \right). \quad (4.35)$$

Here the dislocation is in $+z$ direction, the slip plane is the xz plane, $\rho_i^{(1)}$, $\rho_i^{(2)}$, $\rho_i^{(3)}$ are the edge, vertical, and screw dislocation density at the i -th nodal point, $\rho_i^{(l)} = (f_i^{(l)} - f_{i-1}^{(l)})/(x_i - x_{i-1})$, $l = 1, 2, 3$, $\mathbf{f}_i = (f_i^{(1)}, f_i^{(2)}, f_i^{(3)})$ is the misfit at the i -th nodal, x_i is the position of the i -th nodal, K , $K_s = G/2\pi$ and $K_e = G/[2\pi(1 - \nu)]$ are the energy factors, β is the angle between the dislocation line and the Burgers vector, L is the outer cutoff radius for the elastic energy, $\chi_{ij} = \frac{3}{2}\phi_{i,i-1}\phi_{j,j-1} + \psi_{i-1,j-1} + \psi_{i,j} - \psi_{i,j-1} - \psi_{j,i-1}$ with $\phi_{i,j} = x_i - x_j$ and $\psi_{i,j} = \frac{1}{2}\phi_{i,j}^2 \log |\phi_{i,j}|$, $\gamma_3(\mathbf{f}_i)$ is the generalized stacking fault energy that also includes the misfit in the direction perpendicular to the slip plane, and $(\tau^{(1)}, \tau^{(2)}, \tau^{(3)})$ is the applied stress. It has been shown that the semidiscrete model improves the classic Peierls-Nabarro model significantly by comparing the results with those of the atomistic simulations [72]. This model has been applied to the study of the dislocation properties in aluminum [80]. This model has also been extended to the cross-slip of screw dislocations by considering the distributions of the Burgers vectors in multiple slip planes and the interaction among them [83].

There are also models that consider the nonlocal elasticity in the Peierls-Nabarro framework, for example, Miller *et al* [75] and Picu [82].

5 Dislocation dynamics

The collective motion and interaction of large numbers of dislocations play central roles in the plastic deformation of materials. However, the traditional continuum plasticity theory [89] is not derived quantitatively from the dislocation theory. The direct simulation of dynamics and interactions of dislocations in an elastic continuum, known as the dislocation dynamics, is becoming a more and more important tool for the investigation of the plastic properties of crystals (see, for example, reviews [90–92]). Several dislocation dynamics methods have been developed, and currently the simulations can be performed in a system at the length scales of the order of ten microns and containing a relative large number of dislocations. More efforts are still needed for the method of dislocation dynamics to be a practical engineering tool.

The difficulties in dislocation dynamics come from the fact that various physics at multiple length scales are involved in the evolution of dislocation ensembles. On one hand, the motion and interaction of dislocations at length scales much larger than the atomic size are modeled by the continuum dislocation theory. Even though the interactions between dislocations at such a length scale described well by the continuum theory, they are extraordinarily long-ranged and complicated, depending on the relative positions of all dislocation segments and the orientation of their Burgers vectors and line directions. On the other hand, the short-ranged interactions of dislocations at the atomic length scales, such as the dislocation cross-slip, climb, annihilation, multiplication and reaction, also play important roles in the collective behavior of dislocations.

Early dislocation dynamics models are two-dimensional, focused on either the motion of a single dislocation on the slip plane [93–95], or the motion and interaction of infinitely

long, straight dislocations [96–98]. Recently, Needleman, Van der Giessen and collaborators used two-dimensional dislocation dynamics to examine the applicability of some nonlocal phenomenological continuum plasticity models [99,100], and developed constitutive rules to incorporate three-dimensional dislocation dynamics into two-dimensional simulations [101].

Three-dimensional dislocation dynamics simulations were first performed by Kubin and collaborators [102,103] based upon the front tracking representation for dislocations. This simulation method was augmented later by them and other researchers, for example, [104–122]. In these simulation methods, dislocation lines are discretized into individual segments and each segment is tracked during the evolution of the dislocation microstructures. There are mainly three different discretization methods, including the discretization of dislocations into pure edge and screw segments or segments with a finite set of orientations [102–106,109,113,115], into straight segments with any direction [107,108,110,111,117–120], or into splines [112,114,121]. The long-ranged elastic interaction is modeled by the continuum elasticity theory using the Peach-Koehler formula Eq.(2.17). This long-ranged force is calculated on each dislocation segment, either on the mid-point or the endpoints of the segment, from all other segments at each time increment. Some fast summation methods were proposed [107,109,112]. However, the summation of such kind of forces does not include the line tension effect due to the self interaction of the dislocations. The line tension effect is included either by directly adding the leading order approximation [102–109,113,118] or by a calculation [110–112,114,119,120] using Brown’s splitting and average method [123], i.e., the self stress of a dislocation is approximated by the average of the stress generated by two nearby dislocations separated by a distance of core width (Recall that the self stress is singular). One limitation of the Peach-Koehler formula is that it applies only to isotropic materials. Methods to incorporate anisotropic elasticity into the dislocation dynamics simulations were presented in [117,121]. For the dynamics of dislocations, the dependence of the dislocation velocity v in the slip plane on the resolved shear stress τ is usually modeled by the linear relationship $v = \tau b/B$, where b is the length of the Burgers vector, B is a constant viscous drag coefficient and $1/B$ corresponds to the glide mobility (see Eq.(2.22)) [102–105,107–114,118]. Power laws or the exponential dependence were also used in some models [104,106,119].

Local rules are prescribed to account for the short-ranged reactions of dislocations within a distance less than the core size. Such short-ranged reactions include dislocation annihilation, junction formation, cross-slip of screw segments, etc. The cross-slip of screw segments from one slip plane to another is a thermally activated process, and depends on the atomic structure of the dislocation core and the underlying crystal lattice. A set of local rules were first proposed by Kubin *et al.* [103,104] to incorporate the main properties of cross-slip, with parameters fitted from the experimental results. The cross-slip probability per time step in a recent model [119] is

$$P(L, \delta t) = \beta \frac{L\delta t}{L_0\delta t_0} \exp\left(-\frac{V_{\text{act}}}{kT}(|\tau| - \tau_{III})\right) \quad (5.1)$$

when the Peach-Koehler force on the screw segments projected on the new slip plane is greater than that in the original slip plane. Here β is a normalization constant, V_{act} is an activation volume, k is the Boltzmann constant, T is the temperature, τ is the shear stress, τ_{III} is the stress at which stage-three hardening starts, L is the length of the screw segment that is going to cross-slip, δt is the time step, L_0 and δt_0 are reference values for the length of the cross-slipping segment and for the time step, respectively. Local rules are also prescribed to account for dislocation reaction and junction formation. As described in Section 1, two dislocations with different Burgers vectors \mathbf{b}_1 and \mathbf{b}_2 will react at their junction to form a segment with Burgers vector $\mathbf{b} = \mathbf{b}_1 + \mathbf{b}_2$, if the reaction is energetically favorable. Whether the reaction is energetically favorable or not is determined using the Frank's rule or some more accurate energetic criterion [5]. When the reaction happens, computation nodes are adjusted for the junction, and the formula for the Peach-Koehler force is changed (because the Peach-Koehler force depends on the Burgers vector). Local rules are also needed for dislocation annihilation. There are topological changes associated with the annihilation of two dislocation segments with opposite Burgers vectors. Numerical treatment is needed to determine when the annihilation is going to happen, and then to remove and re-arrange the computation nodes once the annihilation is known to happen. Besides, re-discretization of the dislocations needs to be performed at regular time intervals, to add or remove nodes when the dislocation loops shrink or expand, or when the curvature of the dislocation becomes large near some nodes.

The Peach-Koehler formula Eq.(2.17) used to calculate the stress applies only to dislocations in an infinite medium. For materials with finite size, there is an interaction between dislocations and the material boundaries, resulting in the image force on the dislocations. In these dislocation dynamics models, the boundary conditions on free surfaces were imposed using the idea of superposition of the stress field associated with the dislocations in an infinite elastic medium, and the stress field obtained by solving a complementary problem that enforces the boundary conditions of the finite medium [99, 109, 113, 118, 119]. The complementary problem is usually solved using the finite element method. When dislocations intersect the material boundary, the stress given by the Peach-Koehler formula Eq.(2.17) is singular at the intersecting points where such dislocations terminate. Virtual dislocations were introduced outside the material to make these dislocations form closed loops before the complementary problem is solved [119]. Another type of boundary condition is the periodic boundary condition. The correct and efficient implementation of the image summation of the stress under periodic boundary condition is discussed in [116, 122].

Another class of dislocation dynamics models employ a phase field description of dislocations, as proposed by Khachaturyan *et al* [124, 125] and generalized in [126–129]. In their phase field model, density functions are used to model the evolution of a three-dimensional dislocation system. Dislocation loops are described as the perimeters of thin platelets, which are misfitting coherent inclusions represented by the density functions. The total energy is written as $E = E^{\text{elast}} + E^{\text{cryst}} + E^{\text{grad}}$, where E^{elast} is the elastic energy of the dislocations, E^{cryst} is the crystalline energy modeling the slip systems, and E^{grad} is the gradient energy normally present in phase field models. The crystalline energy

E^{cryst} and the gradient energy E^{grad} are explained to be associated with the dislocation core energy. The elastic energy associated with the dislocations is modeled by the stress field of misfitting inclusions and is calculated using the fast Fourier transform (FFT) under periodic boundary conditions. Since this method is based upon the evolution of a field in the full dimensions of the space, there is no need to track individual dislocation line segments and topological changes occur automatically. However, dislocation climb is not easily incorporated into the current version of their phase field models.

Recently, a three-dimensional level set dislocation dynamics method was proposed by the author and collaborators [18, 130–133]. This simulation method is based on the level set framework proposed by Osher and Sethian [134, 135]. In this level set dislocation dynamics simulation method, dislocation lines in three dimensions are represented as the intersection of zero level sets (or zero contours) of two three-dimensional scalar level set functions. The two three-dimensional level set functions are evolved using a velocity field extended smoothly from the velocity of the dislocation lines. The evolution of the dislocations is implicitly determined by the evolution of the two level set functions. Linear elasticity theory is used to compute the stress field generated by the dislocations. The stress field is solved using an FFT method under periodic boundary conditions. Since the level set method does not track individual dislocation line segments, it easily handles topological changes associated with dislocation multiplication and annihilation. This level set method for dislocation dynamics is capable of simulating the three-dimensional motion of dislocations; naturally accounts for dislocation glide, cross-slip and climb through the choice of the ratio of the glide and climb mobilities. Numerical implementation of the level set method is through simple and accurate finite difference schemes on uniform grids. Results of simulation examples using this method agree very well with the theoretic predictions and the results obtained using other methods [18]. This method has also been used to simulate the dislocation-particle bypass mechanisms [130, 132] and the dislocation dynamics in thin films [133]. Details of this method will be reviewed in the next section.

6 Level set method for dislocation dynamics

In this section, we review the level set dislocation dynamics method and present some of the simulation results. More details of the method and the simulation results can be found in [18, 130–133].

In the level set dislocation dynamics method, dislocations in three-dimensional space $\gamma(t)$ are represented by the intersection of the zero level sets of two level set functions $\phi(x, y, z, t)$ and $\psi(x, y, z, t)$ defined in the three-dimensional space, i.e., where

$$\phi(x, y, z, t) = \psi(x, y, z, t) = 0, \quad (6.1)$$

see Fig.16. The evolution of the dislocations is described by

$$\begin{cases} \phi_t + \mathbf{v} \cdot \nabla \phi = 0 \\ \psi_t + \mathbf{v} \cdot \nabla \psi = 0 \end{cases} \quad (6.2)$$

where \mathbf{v} is the velocity of the dislocation extended smoothly to the three-dimensional space, as described below.

The velocity field of the dislocations is computed from the stress field using Eqs. (2.20) and (2.22). The stress field σ in Eq.(2.20) includes the applied stress field and the stress field generated by the dislocations (self-stress), and is obtained by solving the elasticity system of Eqs. (2.2), (2.3), (2.4), and (2.6). The unit vector locally tangent to the dislocation line, ξ , in Eqs. (2.2) and (2.20), is calculated from the level set functions ϕ and ψ using

$$\xi = \frac{\nabla\phi \times \nabla\psi}{|\nabla\phi \times \nabla\psi|}. \quad (6.3)$$

Under the periodic boundary conditions, the elasticity system for the self-stress can be solved analytically in the Fourier space. In the isotropic medium, Eq.(2.4) is simplified as Eq.(2.5), and the solution of the elasticity system including Eqs. (2.2), (2.3), (2.5), and (2.6) takes the form [18]:

$$\begin{aligned} \hat{\sigma}_{11} &= 2Gi \left(\frac{1}{k_1^2 + k_2^2 + k_3^2} (k_2 b_3 - k_3 b_2) \hat{d}_1 \right. \\ &\quad \left. - \frac{1}{1-\nu} \frac{k_2^2 + k_3^2}{(k_1^2 + k_2^2 + k_3^2)^2} [(k_2 b_3 - k_3 b_2) \hat{d}_1 + (k_3 b_1 - k_1 b_3) \hat{d}_2 + (k_1 b_2 - k_2 b_1) \hat{d}_3] \right) \\ \hat{\sigma}_{22} &= 2Gi \left(\frac{1}{k_1^2 + k_2^2 + k_3^2} (k_3 b_1 - k_1 b_3) \hat{d}_2 \right. \\ &\quad \left. - \frac{1}{1-\nu} \frac{k_1^2 + k_3^2}{(k_1^2 + k_2^2 + k_3^2)^2} [(k_2 b_3 - k_3 b_2) \hat{d}_1 + (k_3 b_1 - k_1 b_3) \hat{d}_2 + (k_1 b_2 - k_2 b_1) \hat{d}_3] \right) \\ \hat{\sigma}_{33} &= 2Gi \left(\frac{1}{k_1^2 + k_2^2 + k_3^2} (k_1 b_2 - k_2 b_1) \hat{d}_3 \right. \\ &\quad \left. - \frac{1}{1-\nu} \frac{k_1^2 + k_2^2}{(k_1^2 + k_2^2 + k_3^2)^2} [(k_2 b_3 - k_3 b_2) \hat{d}_1 + (k_3 b_1 - k_1 b_3) \hat{d}_2 + (k_1 b_2 - k_2 b_1) \hat{d}_3] \right) \\ \hat{\sigma}_{12} &= \hat{\sigma}_{21} = 2Gi \left(\frac{1}{2(k_1^2 + k_2^2 + k_3^2)} [(k_3 b_1 - k_1 b_3) \hat{d}_1 + (k_2 b_3 - k_3 b_2) \hat{d}_2] \right. \\ &\quad \left. + \frac{1}{1-\nu} \frac{k_1 k_2}{(k_1^2 + k_2^2 + k_3^2)^2} [(k_2 b_3 - k_3 b_2) \hat{d}_1 + (k_3 b_1 - k_1 b_3) \hat{d}_2 + (k_1 b_2 - k_2 b_1) \hat{d}_3] \right) \\ \hat{\sigma}_{23} &= \hat{\sigma}_{32} = 2Gi \left(\frac{1}{2(k_1^2 + k_2^2 + k_3^2)} [(k_1 b_2 - k_2 b_1) \hat{d}_2 + (k_3 b_1 - k_1 b_3) \hat{d}_3] \right. \\ &\quad \left. + \frac{1}{1-\nu} \frac{k_2 k_3}{(k_1^2 + k_2^2 + k_3^2)^2} [(k_2 b_3 - k_3 b_2) \hat{d}_1 + (k_3 b_1 - k_1 b_3) \hat{d}_2 + (k_1 b_2 - k_2 b_1) \hat{d}_3] \right) \\ \hat{\sigma}_{13} &= \hat{\sigma}_{31} = 2Gi \left(\frac{1}{2(k_1^2 + k_2^2 + k_3^2)} [(k_1 b_2 - k_2 b_1) \hat{d}_1 + (k_2 b_3 - k_3 b_2) \hat{d}_3] \right. \\ &\quad \left. + \frac{1}{1-\nu} \frac{k_1 k_3}{(k_1^2 + k_2^2 + k_3^2)^2} [(k_2 b_3 - k_3 b_2) \hat{d}_1 + (k_3 b_1 - k_1 b_3) \hat{d}_2 + (k_1 b_2 - k_2 b_1) \hat{d}_3] \right) \end{aligned} \quad (6.4)$$

where $\hat{\sigma}_{ij}$ is the Fourier coefficient for the frequency (k_1, k_2, k_3) for the self-stress σ_{ij} , $i, j = 1, 2, 3$, \hat{d}_1 , \hat{d}_2 and \hat{d}_3 are the Fourier coefficients for the frequency (k_1, k_2, k_3) for the

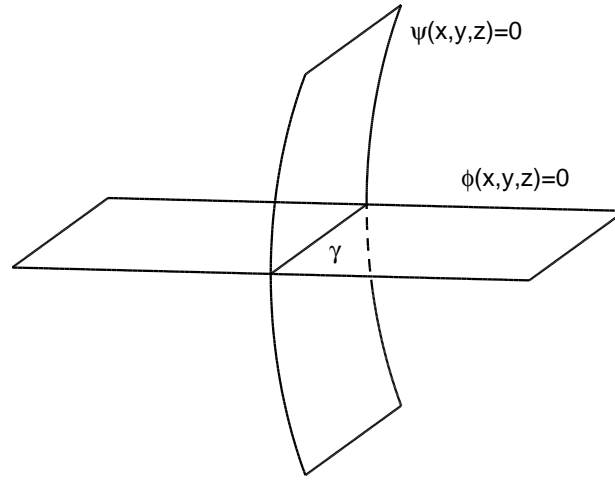


Figure 16: Dislocations in three dimensional space $\gamma(t)$ are the intersection of the zero level sets of the two level set functions $\phi(x, y, z, t)$ and $\psi(x, y, z, t)$.

three components of $\xi\delta(\gamma)$ in Eq.(2.2), respectively, and b_1, b_2, b_3 are the three components of the Burgers vector \mathbf{b} . A similar expression can be obtained for the anisotropic elasticity. A constant applied stress field can be added to total stress field in Eq.(2.20). The boundary effect can be included by solving for the image force field using the method of Green's function for half-space medium [133], or using the finite element method for materials with general-shape boundaries. Note that the obtained velocity field is defined in the whole medium, which is a natural extension of the velocity field in the evolution equations for the level set functions Eq.(6.2).

As discussed before, the self-stress obtained by the linear elasticity theory is singular on the dislocation lines, which is because the linear elasticity theory does not apply in the core region of the dislocation. To handle this problem, we use a smeared delta function instead of the exact one in Eq.(2.2). The smeared delta function is defined in the plane perpendicular to the dislocation line, and the vector ξ is defined everywhere inside the dislocation core to be the dislocation line tangent vector. This smeared delta function can be considered to be the distribution of the Burgers vector in the core region of the dislocation. More precisely, the smeared delta function in Eq. (2.2) is given by

$$\delta(\gamma) = \delta(\phi)\delta(\psi), \tag{6.5}$$

where the delta function on the right-hand side is one-dimensional, smeared delta function

$$\delta(x) = \begin{cases} \frac{1}{2\epsilon} \left(1 + \cos \frac{\pi x}{\epsilon}\right) & -\epsilon \leq x \leq \epsilon, \\ 0 & \text{otherwise,} \end{cases} \tag{6.6}$$

and ϵ scales the distance over which the delta function is smeared. The level set functions ϕ and ψ are usually chosen to be signed distance functions to their zero level sets,

respectively, and their zero level sets are kept perpendicular to each other (A numerical procedure called reinitialization is used to retain these properties of ϕ and ψ during their temporal evolution, as will be discussed below). Therefore the delta function defined by (6.5) is a two dimensional smeared delta function in the plane perpendicular to the dislocation line. Moreover, the size and the shape of the core region does not change during the evolution of the dislocation microstructure.

We now define the mobility tensor \mathbf{M} as

$$\mathbf{M} = \begin{cases} m_g(\mathbf{I} - \mathbf{n} \otimes \mathbf{n}) + m_c \mathbf{n} \otimes \mathbf{n} & \text{non-screw } (\xi \text{ not parallel to } \mathbf{b}) \\ m_g \mathbf{I} & \text{screw } (\xi \text{ parallel to } \mathbf{b}) \end{cases}, \quad (6.7)$$

where

$$\mathbf{n} = \frac{\xi \times \mathbf{b}}{|\xi \times \mathbf{b}|} \quad (6.8)$$

is the unit vector normal to the slip plane (i.e., the plane that contains the tangent vector ξ of the dislocation and its Burgers vector \mathbf{b}), \mathbf{I} is the identity matrix, $\mathbf{I} - \mathbf{n} \otimes \mathbf{n}$ is the projection matrix that projects vectors onto the plane with normal vector \mathbf{n} , m_g is the mobility constant for dislocation glide and m_c is the mobility constant for dislocation climb. Typically,

$$0 \leq \frac{m_c}{m_g} \ll 1. \quad (6.9)$$

The mobility tensor \mathbf{M} , defined above, can account for the relatively high glide mobility and slow climb mobility discussed in Section 1. This mobility does not include the effect of crystallography, namely the non-screw dislocation segments can move in any plane containing its line direction and Burgers vector, and the screw segments can move in any plane. This kind of motion applies to dislocations in BCC crystals. In FCC crystals, the motion of dislocations are restricted to some particular slip planes in which the motion of dislocations is energetically favorable, see Section 3. Another form of mobility tensor is used for dislocations in FCC crystals [133]. Besides, in Eq.(6.7), the cross-slip of screw segments happens without thermal activation, which again applies to dislocations in BCC crystals. A probability form of the cross-slip mobility incorporating the thermal activation process was used in [133]. More accurate dependence of the mobility on temperature or dislocation line direction can be included, and more accurate power law or exponential dependence between the dislocation velocity and the force acting on dislocations can be adopted, when they are necessary.

The intersection of the zero level sets of the two level set functions ϕ and ψ can be multiple lines, therefore multiple dislocations can be represented using these two level set functions. The above description of the method applies to the case where all dislocations have the same Burgers vector \mathbf{b} . The symbol γ in Eq.(2.2) actually represents all of the dislocations with Burgers vector \mathbf{b} . For a more general case when dislocation lines have different Burgers vectors, we can use different level set functions ϕ_i and ψ_i for each possible Burgers vector \mathbf{b}_i , $i = 1, 2, \dots, N$, where N is the total number of the possible

Burgers vectors, and

$$\nabla \times \mathbf{w} = \sum_{i=1}^N \xi_i \delta(\gamma_i) \otimes \mathbf{b}_i \quad (6.10)$$

instead of Eq.(2.2) in the elasticity system. Here γ_i represents all of the dislocations with Burgers vector \mathbf{b}_i , and ξ_i is the tangent direction of such a dislocation.

For the numerical implementation, the self-stress field is obtained by the FFT approach using Eq.(6.4). The core radius of the delta function (6.6) is $\epsilon = 3dx$, where dx is the spacing of the numerical grid. For the mobility tensor (6.7), we use the mobility for a screw dislocation when $|\xi \times \mathbf{b}| < 0.1$ and use the mobility for a non-screw dislocation otherwise.

The level set evolution equations are commonly solved using high order ENO (essentially nonoscillatory) [134, 136] or WENO (weighted essentially nonoscillatory) methods [137] for the spatial discretization, and TVD (total variation diminishing) Runge-Kutta methods [138, 139] for the temporal discretization.

To reduce the numerical errors, a standard level set technique called reinitialization [135, 140–142] is used to reconstruct new level set functions from old ones with the dislocations unchanged, so that the level set functions are always signed distance functions from their own zero level sets and their zero level sets are perpendicular to each other locally near the dislocations.

We use a smeared delta function (rather than an exact delta function) to compute the self-stress of the dislocations in order to smooth the singularity in the dislocation self-stress. The leading order of the self-stress near the dislocations, when using a smeared delta function, is of the order $1/\epsilon$, where ϵ is the dislocation core size. This $\mathcal{O}(1/\epsilon)$ self-stress near the dislocations does not contribute to the motion of the dislocations. We remove this contribution to the self-stress by a procedure which we call velocity interpolation and extension. We first interpolate the velocity and the tangent vector on the dislocation line and then extend the interpolated values to the whole space using the fast sweeping method [143–147]. Another advantage of this procedure is that it gives a more accurate value of the tangent vector of the dislocations, which is crucial to determine the slip plane and the mobility of dislocations (Eq.(6.7)).

Figs. 17-23 show several applications of the level set method for dislocation dynamics. The simulations were performed within simulation cells that were $l \times l \times l$ (where $l = 2$). The simulation cell is discretized into $64 \times 64 \times 64$ grid points (For Figs. 18 and 23, the simulation cell is $2l \times 2l \times l$ discretized into $128 \times 128 \times 64$ grid points). Isotropic elasticity is used and the Poisson ratio $\nu = 1/3$. The climb mobility $m_c = 0$, except in Figs. 17 and 22. The units and other parameters in these simulations can be found in [18, 130].

Fig. 17 shows an initially circular glide loop expanding under a complex applied stress with mobility ratios m_c/m_g of 0, 0.25, and 1.0, where m_c and m_g are the climb mobility and glide mobility, respectively. The applied stress generates a finite force on all the dislocation segments that tends to move them out of the initial slip plane. However, if the climb mobility $m_c = 0$, only the screw segments move out of the slip plane; the non-

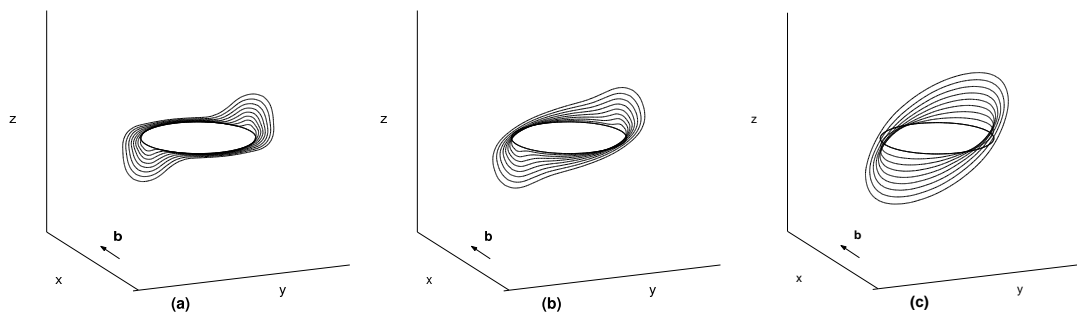


Figure 17: An initially circular glide loop in the xy plane, with a Burgers vector \mathbf{b} in the x direction, expanding under a complex applied stress ($\sigma_{xz}, \sigma_{xy} \neq 0$) with mobility ratios m_c/m_g of (a) 0, (b) 0.25, and (c) 1.0. The loop is plotted at regular intervals in time.

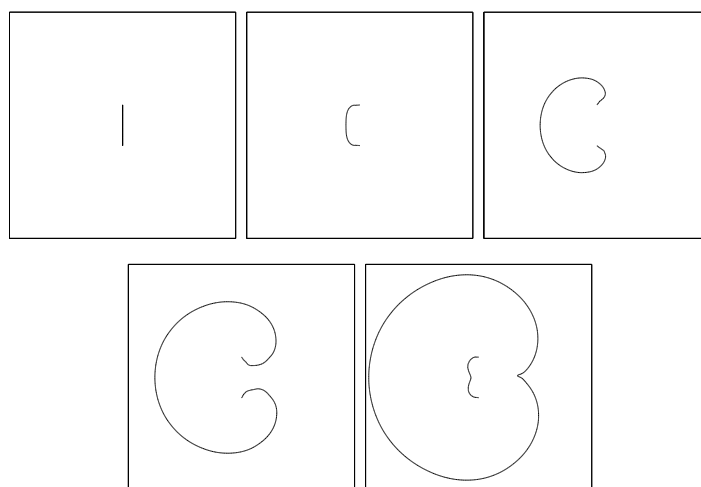


Figure 18: Simulation of the Frank-Read source. Initially the dislocation segment is an edge segment in the xy plane (the z axis is pointing out of the paper). The Burgers vector is parallel to the x axis and a stress σ_{xz} is applied. The configuration in the slip plane is plotted at different time during the evolution.

screw segments cannot because the mobility in such direction is zero (Fig. 17(a)). If the climb mobility $m_c > 0$, both the screw and non-screw segments move out of the slip plane (Fig. 17(b) and (c)).

Fig. 18 shows the simulation of the Frank-Read source [11]. Initially the dislocation segment is an edge segment. It bends out under an applied stress and generates a new loop outside. The initial configuration in this simulation is a rectangular loop in a plane perpendicular to the paper. Of its four segments, two opposite ones are operating as the Frank-Read sources in the planes perpendicular to the initial loop (one is shown above), and the other two are fixed.

Fig. 19 shows an edge dislocation bypassing a linear array of impenetrable particles, leaving Orowan loops [148] around the particles behind. The dislocation moves towards the particles under an applied stress. The glide plane of the dislocation intersects the

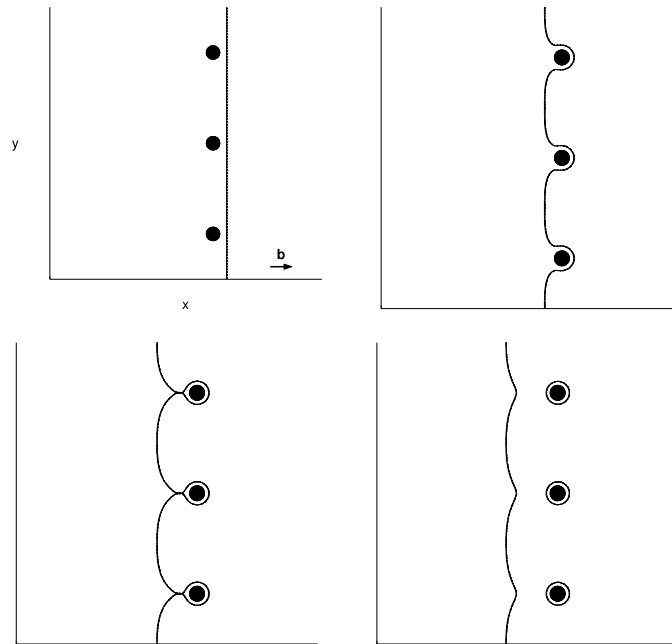


Figure 19: An edge dislocation bypassing a linear array of impenetrable particles, leaving Orowan loops around the particles behind. The Burgers vector \mathbf{b} is in the x direction. The applied stress $\sigma_{xz} \neq 0$, where the z direction is pointing out of the paper.

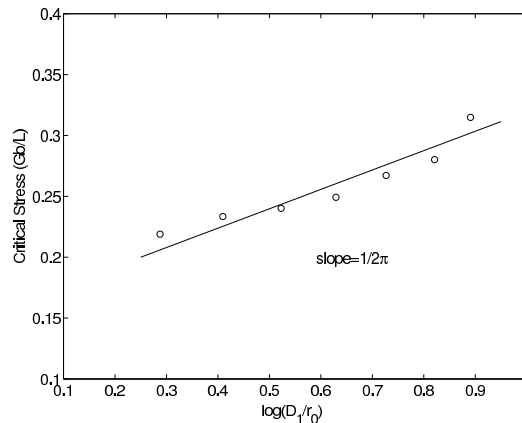


Figure 20: The critical stress for an edge dislocation to bypass co-planar impenetrable particles by the Orowan loop mechanism. The stress is plotted in the unit Gb/L against $\log(D_1/r_0)$.

centers of the particles (i.e., the particles are coplanar). The impenetrable particles are assumed to exert a strong short-range repulsive force on dislocations.

Fig. 20 shows the critical stress for an edge dislocation to bypass coplanar impenetrable particles by the Orowan loop mechanism. The stress is plotted in the unit Gb/L against $\log(D_1/r_0)$, where G is the shear modulus, b is the length of the Burgers vector, L is the

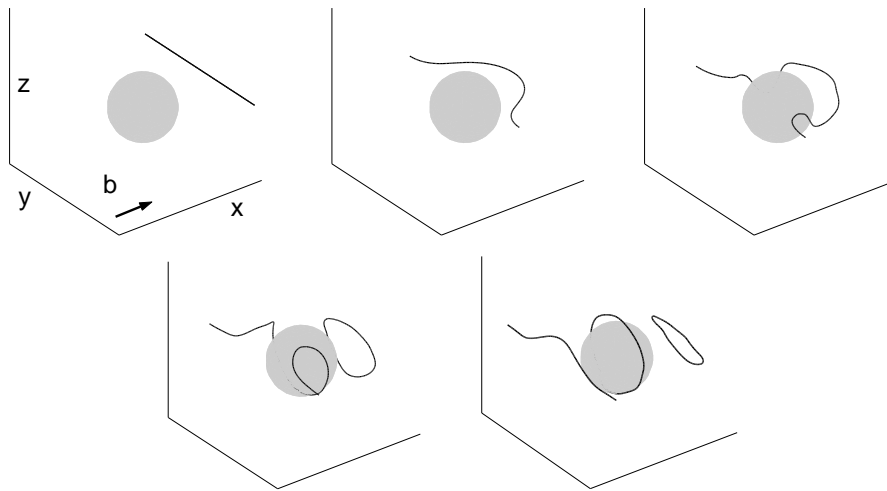


Figure 21: An edge dislocation bypassing a misfitting impenetrable spherical particle by cross-slip, where the slip plane of the dislocation is above the particle center. The Burgers vector \mathbf{b} is in the x direction, the applied stress is $\sigma_{xz} \neq 0$. The misfit $\epsilon_{\text{mis}} > 0$.

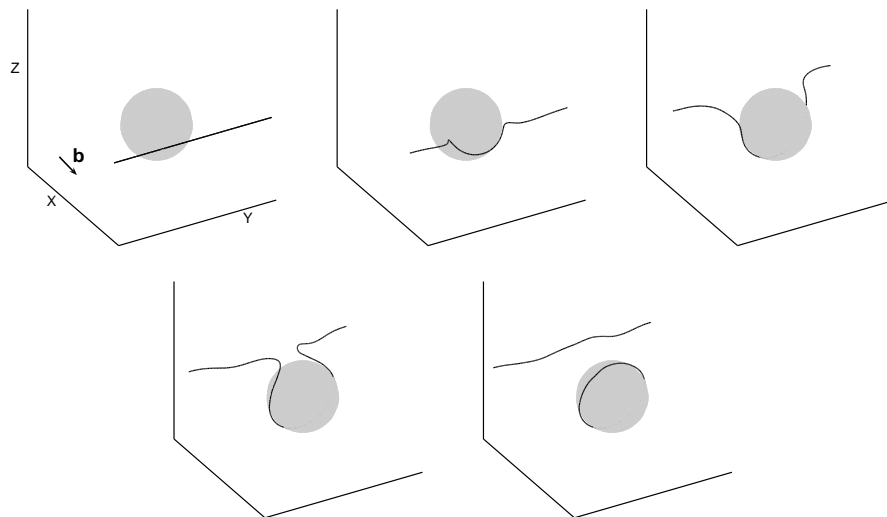


Figure 22: An edge dislocation bypassing a misfitting impenetrable particle under the condition that the ratio of the climb mobility over the glide mobility is $m_c/m_g = 0.1$. The slip plane of the dislocation is above the particle center. The Burgers vector \mathbf{b} is in the x direction, the applied stress is $\sigma_{xz} \neq 0$. The misfit $\epsilon_{\text{mis}} > 0$.

inter-particle distance, D is the diameter of the particle, D_1 is the harmonic mean of L and D , and r_0 is the inner cut-off radius associated with the dislocation core. The data points represent the simulation results and the straight line is the best fit to our data using the classic equation $\frac{Gb}{2\pi L} \log \frac{D_1}{r_0}$ [95, 148, 149]. It shows a good agreement between the simulation results using the level set method and the theoretical estimates.

Fig. 21 shows an edge dislocation bypassing a misfitting impenetrable spherical particle

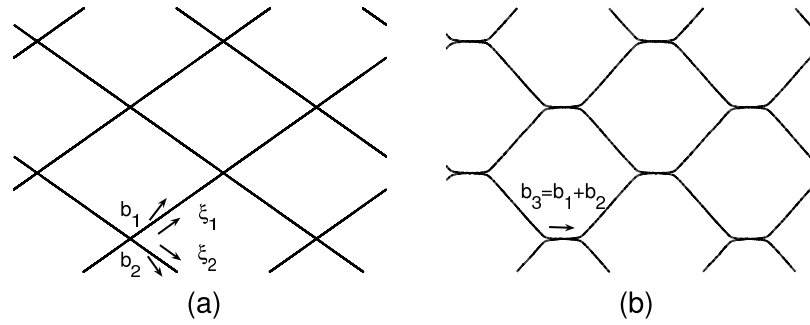


Figure 23: Dislocation model for a grain boundary in a BCC crystal. (a) Unstable network. (b) Stable hexagonal network formed by reaction of dislocations.

by cross-slip [150], where the slip plane of the dislocation intersects the particle above the particle center. The misfit $\epsilon_{\text{mis}} > 0$. The displacement and stress fields generated by a (dilatational) misfitting spherical particle (isotropic elasticity) can be found in [151, 152]. In the simulation, the dislocation moves towards the particles under an applied stress. Two loops are left behind: one is behind the particle and the other is around the particle. They have the same Burgers vector but opposite line directions.

Fig. 22 shows the same edge dislocation bypassing the same misfitting impenetrable particle, except that now the dislocation climb is included by setting $m_c/m_g = 0.1$, where m_c and m_g are the climb mobility and glide mobility, respectively. The dislocation segment behind the particle climbs down to the bottom of the particle and only one loop is left around the particle. More simulation results on the climb effect can be found in [131].

Fig. 23 shows a dislocation model for a grain boundary [5, 6, 153] in a BCC crystal (the dislocations in four simulation cells are shown). The grain boundary is a dislocation network in a (110) plane. Initially, the network consists of two sets of straight dislocations, one set of dislocations are in the $\xi_1 = \frac{1}{\sqrt{6}}[1\bar{1}2]$ direction with Burgers vector $\mathbf{b}_1 = \frac{1}{2}[1\bar{1}1]$, the other set of dislocations are in the $\xi_2 = \frac{1}{\sqrt{6}}[\bar{1}12]$ direction with Burgers vector $\mathbf{b}_2 = \frac{1}{2}[\bar{1}11]$, see Fig. 23(a). However, this network is unstable. Because if $\mathbf{b}_3 = \mathbf{b}_1 + \mathbf{b}_2 = [001]$, we have $b_3^2 < b_1^2 + b_2^2$, and from Frank's rule the two dislocations with Burgers vectors \mathbf{b}_1 and \mathbf{b}_2 , respectively, will react to form one single dislocation with Burgers vector \mathbf{b}_3 . On the other hand, the reaction increases the total length and therefore the total energy of the dislocations. A stable hexagonal net is formed under these two effects, see Fig. 23(b). This simulation result agrees with the theoretic prediction [5, 6, 153].

Acknowledgments

This work is supported by Hong Kong RGC Competitive Earmarked Research Grant 604604 and DAG 03/04.SC23.

References

- [1] V. Volterra, *Ann. Ec. Norm. Super.*, 24 (1907), 401.
- [2] G.I. Taylor, *Proc. Roy. Soc.*, A145 (1934), 362.
- [3] E. Orowan, *Z. Phys.*, 89 (1934), 634.
- [4] M. Polanyi, *Z. Phys.*, 89 (1934), 660.
- [5] J.P. Hirth, J. Lothe, *Theory of Dislocations*, 2nd ed., John Wiley, New York, 1982.
- [6] F.R.N. Nabarro, *Theory of Crystal Dislocations*, Clarendon Press, Oxford, England, 1967.
- [7] F.R.N. Nabarro (Ed.), *Dislocations in Solids*, Vol.1-9, F.R.N. Nabarro and M.S. Duesbery (Eds.), Vol.10-11, F.R.N. Nabarro and J.P. Hirth (Eds.), Vol.12, North Holland, Amsterdam, 1979-2004.
- [8] J. Frenkel, *Z. Phys.*, 37 (1926), 572.
- [9] J.M. Burgers, *Proc. Roy. Acad. Sci, Amsterdam*, 42 (1939), 293 and 378; *Proc. Phys. Soc.*, 52 (1940), 23.
- [10] F.C. Frank, *Physica*, 15 (1949), 131.
- [11] F.C. Frank, W.T. Read, *Phys. Rev.*, 79 (1950), 722.
- [12] D. Hull, D.J. Bacon, *Introduction to Dislocations*, 4th ed., Butterworth-Heinemann, Oxford, 2001.
- [13] J. Weertman, J.R. Weertman, *Elementary Dislocation Theory*, Oxford University Press, New York, 1992.
- [14] R.W. Lardner, *Mathematical Theory of Dislocations and Fracture*, University of Toronto Press, Toronto and Buffalo, 1974.
- [15] L.D. Landau, E.M. Lifshitz, *Theory of Elasticity*, 3rd ed., Butterworth-Heinemann, Oxford, 1986.
- [16] M. Peach, J.S. Koehler, *Phys. Rev.*, 80 (1950), 436.
- [17] J. Blin, *Acta Met.*, 3 (1955), 199.
- [18] Y. Xiang, L.T. Cheng, D.J. Srolovitz, W. E, *Acta Mater.*, 51 (2003), 5499.
- [19] W.G. Johnston, J.J. Gilman, *J. Appl. Phys.*, 30 (1959), 129.
- [20] D.F. Stein, J.R. Low, *J. Appl. Phys.*, 31 (1960), 362.
- [21] J.J. Gilman, *Aust. J. Phys.*, 13 (1960), 327.
- [22] J.W. Christian, V. Vitek, *Rep. Prog. Phys.*, 33 (1970), 307.
- [23] S. Amelinckx, in: F.R.N. Nabarro (Ed.), *Dislocations in Solids*, Vol.2, North-Holland, Amsterdam, 1979.
- [24] R. Bullough, V.K. Tewary, in: F.R.N. Nabarro (Ed.), *Dislocations in Solids*, Vol.2, North-Holland, Amsterdam, 1979.
- [25] M.P. Puls, in: M.F. Ashby, R. Bullough, C.S. Hartley, J.P. Hirth (Eds.), *Dislocation Modeling of Physical Systems*, Pergamon, New York, 1981.
- [26] M.S. Duesbery, G.Y. Richardson, *CRC Crit. Rev. Solid State Mater. Sci.*, 17 (1991), 1.
- [27] V. Vitek, *Prog. Mater. Sci.*, 36 (1992), 1.
- [28] J.A. Moriarty, V. Vitek, V.V. Bulatov, S. Yip, *J. Comput.-Aided Mater. Design*, 9 (2002), 99.
- [29] W. Cai, V.V. Bulatov, J. Chang, J. Li, S. Yip, in: F.R.N. Nabarro, J.P. Hirth (Eds.), *Dislocations in Solids*, Vol.12, North-Holland, Amsterdam, 2004.
- [30] R.D. Heidenreich, W. Shockley, in: *Report of a Conference on Strength of Solids*, Physical Society, London, 1948, p.57.
- [31] F.C. Frank, *Proc. Phys. Soc.*, 62A (1949), 202; F.C. Frank, J.F. Nicholas, *Phil. Mag.*, 44 (1953), 1213.

- [32] V.V. Bulatov, W. Cai, *Computer Simulation of Dislocations*, Oxford University Press, in preparation.
- [33] V.V. Bulatov, S. Yip, A.S. Argon, *Phil. Mag. A*, 72 (1995), 453.
- [34] T. Rasmussen, K.W. Jacobsen, T. Leffers, O.B. Pedersen, *Phys. Rev. B*, 56 (1997), 2977.
- [35] M.S. Duesbery, V. Vitek, *Acta Mater.*, 46 (1998), 1481.
- [36] M.S. Duesbery, *Modelling Simul. Mater. Sci. Eng.*, 6 (1998), 35.
- [37] D. Rodney, R. Phillips, *Phys. Rev. Lett.*, 82 (1999), 1704.
- [38] V.V. Bulatov, O. Richmond, M.V. Glazov, *Acta Mater.*, 47 (1999), 3507.
- [39] S. Ismail-Beigi, T.A. Arias, *Phys. Rev. Lett.*, 84 (2000), 1499.
- [40] C. Woodward, S.I. Rao, *Phil. Mag. A*, 81 (2001), 1305; S.I. Rao, C. Woodward, *Phil. Mag. A*, 81 (2001), 1317.
- [41] J. Marian, W. Cai, V.V. Bulatov, *Nature Materials*, 3 (2004), 158.
- [42] D.L. Olmsted, L.G. Hector, W.A. Curtin, R.J. Clifton, *Modelling Simul. Mater. Sci. Eng.*, 13 (2005), 371.
- [43] M.S. Daw, M.I. Baskes, *Phys. Rev. Lett.*, 45 (1984), 6443.
- [44] F. Ercolessi, J.B. Adams, *Europhys. Lett.*, 26 (1994), 583.
- [45] J.E. Sinclair, R. Fletcher, *J. Phys. C*, 7 (1974), 864.
- [46] V.B. Shenoy, R.V. Kukta, R. Phillips, *Phys. Rev. Lett.*, 84 (2000), 1491.
- [47] M. de Koning, W. Cai, V.V. Bulatov, *Phys. Rev. Lett.*, 91 (2003), 025503.
- [48] R. Peierls, *Proc. Phys. Soc.*, 52 (1940), 34.
- [49] F.R.N. Nabarro, *Proc. Phys. Soc.*, 59 (1947), 256.
- [50] F.R.N. Nabarro, *Mat. Sci. Eng. A*, 234-236 (1997), 67; *Phil. Mag. A*, 75 (1997), 703.
- [51] A.H. Cottrell, F.R.N. Nabarro, in: A.H. Cottrell, *Dislocations and Plastic Flow in Crystals*, Oxford University Press, 1953.
- [52] J.D. Eshelby, *Phil. Mag.*, 40 (1949), 903.
- [53] G. Leibfried and K. Lucke, *Z. Phys.*, 126 (1949), 450.
- [54] A.J. Foreman, M.A. Jaswon, J.K. Wood, *Proc. Phys. Soc.*, 64A (1951), 156.
- [55] G. Leibfried, H.D. Dietze, *Z. Phys.*, 131 (1951), 113.
- [56] H.D. Dietze, *Z. Phys.*, 132 (1952), 107.
- [57] A.H. Cottrell, *Dislocations and Plastic Flow in Crystals*, Oxford University Press, 1953.
- [58] A. Seeger, G. Schoeck, *Acta Metall.*, 1 (1953), 519.
- [59] H.B. Huntington, *Proc. Phys. Soc.*, 68B (1955), 1043.
- [60] D. Kuhlmann-Wilsdorf, *Phys. Rev.*, 120 (1960), 773.
- [61] V. Vitek, L. Lejcek, D.K. Bowen, in: P.C. Gehlen, J.R. Beeler Jr., R.I. Jaffee (Eds.), *Proceedings of Battelle Colloquium on Interatomic Potentials and Simulation of Lattice Defects*, Plenum Press, New York, 1972.
- [62] L. Lejcek, *Czech. J. Phys. B*, 22 (1972), 802; F. Kroupa, L. Lejcek, *Czech. J. Phys. B*, 22 (1972), 813.
- [63] A.M. Kosevich, in: F.R.N. Nabarro (Ed.), *Dislocations in Solids*, Vol. 1, North-Holland, Amsterdam, 1979.
- [64] E. Kaxiras, M.S. Duesbery, *Phys. Rev. Lett.*, 70 (1993), 3752.
- [65] K. Ohsawa, H. Koizumi, H.O.K. Kirchner, T. Suzuki, *Phil. Mag. A*, 69 (1994), 171.
- [66] B. Joos, Q. Ren, M.S. Duesbery, *Phys. Rev. B*, 50 (1994), 5890; Q. Ren, B. Joos, M.S. Duesbery, *Phys. Rev. B*, 52 (1995), 13223.
- [67] G. Schoeck, *Phil. Mag. A*, 69 (1994), 1085; *Acta Mater.*, 45 (1997), 2597; *Phil. Mag. Lett.*, 76 (1997), 15; *Mater. Sci. Eng. A*, 241 (1998), 14; *Phil. Mag. A*, 81 (2001), 1161; *Comput. Mater. Sci.*, 21 (2001), 124; *Phil. Mag. A*, 82 (2002), 1033; *Mater. Sci. Eng. A*, 400-401 (2005), 7.

- [68] J.N. Wang, *Acta Mater.*, 44 (1996), 1541; *Mater. Sci. Eng. A*, 206 (1996), 259.
- [69] Y.M. Juan, E. Kaxiras, *Phil. Mag. A*, 74 (1996), 1367.
- [70] N.I. Medvedeva, O.N. Mryasov, Yu. N. Gornostyrev, D.L. Novikov, A.J. Freeman, *Phys. Rev. B.*, 54 (1996), 13506; O.N. Mryasov, Yu. N. Gornostyrev, A.J. Freeman, *Phys. Rev. B.*, 58 (1998), 11927.
- [71] B. Joos, M.S. Duesbery, *Phys. Rev. Lett.*, 78 (1997), 266.
- [72] V.V. Bulatov, E. Kaxiras, *Phys. Rev. Lett.*, 78 (1997), 4221.
- [73] J. Hartford, B. von Sydow, G. Wahnstrom, B.I. Lundqvist, *Phys. Rev. B.*, 58 (1998), 2487.
- [74] A.B. Movchan, R. Bullough, J.R. Willis, *Euro. J. Appl. Math.*, 9 (1998), 373.
- [75] R. Miller, R. Phillips, G. Beltz, M. Ortiz, *J. Mech. Phys. Solids*, 46 (1998), 1845.
- [76] G. Schoeck, *Phys. Rev. Lett.*, 82 (1999), 2310.
- [77] G. Schoeck, *Phil. Mag. A*, 79 (1999), 2629.
- [78] B. von Sydow, J. Hartford, G. Wahnstrom, *Comput. Mater. Sci.*, 15 (1999), 367.
- [79] A.H.W. Ngan, *Phil. Mag. A*, 79 (1999), 1697.
- [80] G. Lu, N. Kioussis, V.V. Bulatov, E. Kaxiras, *Phys. Rev. B*, 62 (2000), 3099; *Mat. Sci. Eng. A*, 309-310 (2001), 142.
- [81] B. Joos, J. Zhou, *Phil. Mag. A*, 81 (2001), 1329.
- [82] R.C. Picu, *J. Mech. Phys. Solids*, 50 (2002), 717; 1923.
- [83] G. Lu, V.V. Bulatov, N. Kioussis, *Phys. Rev. B*, 66 (2002), 144103; *Phil. Mag.*, 83 (2003), 3539.
- [84] G. Schoeck, M. Krystian, *Phil. Mag.*, 85 (2005), 949.
- [85] V. Vitek, *Phil. Mag.*, 18 (1968), 773; *Crystal Lattice Defects*, 5 (1974), 1;
- [86] J.D. Eshelby, W.T. Read, W. Shockley, *Acta Met.*, 1 (1953), 251.
- [87] A.J.E. Foreman, *Acta Met.*, 3 (1955), 322.
- [88] A.N. Stroh, *Phil. Mag.*, 3 (1958), 625.
- [89] A.S. Khan, S. Huang, *Continuum Theory of Plasticity*, John Wiley & Sons, New York, 1995.
- [90] B. Devincere, L.P. Kubin, C. Lemarchand, R. Madec, *Mat. Sci. Eng. A*, 309 (2001), 211.
- [91] V.V. Bulatov, *J. Comput.-Aided Mater. Design*, 9 (2002), 133.
- [92] H.M. Zbib and T.A. Khraishi, p.1097; E. Van der Giessen, A. Needleman, p.1115; N.M. Ghoniem, p.2269; Y.U. Wang, Y.M. Jin, A.G. Khachaturyan, p.2287; Y. Xiang and D.J. Srolovitz, p.2307, in: S. Yip (Ed.), *Handbook of Materials Modeling, Vol.1, Methods and Models of Materials Modeling*, Springer, 2005.
- [93] A.J.E. Foreman, M.J. Makin, *Phil. Mag.*, 14 (1966), 911.
- [94] D.J. Bacon, *Physica Status Solidi*, 23 (1967), 527.
- [95] D.J. Bacon, U.F. Kocks, R.O. Scattergood, *Phil. Mag.*, 28 (1973), 1241.
- [96] J. Lepinoux, L.P. Kubin, *Scripta Met.*, 21 (1987), 833.
- [97] N.M. Ghoniem, R.J. Amodeo, *Solid State Phenomena*, 3&4 (1988), 377.
- [98] A.N. Gulluoglu, D.J. Srolovitz, R. LeSar, P.S. Lomdahl, *Scripta Met.*, 23 (1989), 1347.
- [99] E. Van der Giessen, A. Needleman, *Modelling Simul. Mater. Sci. Eng.*, 3 (1995), 689.
- [100] A. Needleman, E. Van der Giessen, *Modelling Simul. Mater. Sci. Eng.*, 309-310 (2001), 1; *Key Eng. Mat.*, 233 (2003), 13; E. Bittencourt, A. Needleman, M.E. Gurtin, E. Van der Giessen, *J. Mech. Phys. Solids*, 51 (2003), 281.
- [101] A.A. Benzerga, Y. Brechet, A. Needleman, E. Van der Giessen, *Modelling Simul. Mater. Sci. Eng.*, 12 (2004), 159.
- [102] L.P. Kubin, G.R. Canova, in: U. Messerschmidt, et al. (Eds.), *Electron Microscopy in Plasticity and Fracture Research of Materials*, Akademie Verlag, Berlin, 1990, p.23.
- [103] L.P. Kubin, G. Canova, M. Condat, B. Devincere, V. Pontikis, Y. Brechet, *Solid State Phe-*

- nomena, 23/24 (1992), 455.
- [104] B. Devincere, in: H.O. Kirchner, V. Pontikis, L.P. Kubin (Eds.), *Computer Simulation in Materials Science*, North-Holland, Amsterdam, 1996, p.309.
 - [105] A. Moulin, M. Condat, L.P. Kubin, *Acta Mater.*, 45 (1997), 2339.
 - [106] M. Tang, L.P. Kubin, G.R. Canova, *Acta Mater.*, 46 (1998), 3221.
 - [107] H.M. Zbib, M. Rhee, J.P. Hirth, *Int. J. Mech. Sci.*, 40 (1998), 113.
 - [108] M. Rhee, H.M. Zbib, J.P. Hirth, H. Huang, T. de la Rubia, *Modelling Simul. Mater. Sci. Eng.*, 6, (1998), 467.
 - [109] M. Verdier, M. Fivel, I. Groma, *Modelling Simul. Mater. Sci. Eng.*, 6, (1998), 755.
 - [110] R.V. Kukta, L.B. Freund, in: V.V. Bulatov, T. Diaz de la Rubia, R. Phillips, E. Kaxiras, N. Ghoniem (Eds.), *Multiscale Modelling of Materials*, Materials Research Society, Boston, 1999, p.99.
 - [111] K.W. Schwarz, *J. Appl. Phys.*, 85 (1999), 108.
 - [112] N.M. Ghoniem, L.Z. Sun, *Phys. Rev. B*, 60 (1999), 128.
 - [113] M.C. Fivel, A.A. El-Azab, *J. Phys. IV*, 9, (1999), Pr9-261.
 - [114] N.M. Ghoniem, S.H. Tong, L.Z. Sun, *Phys. Rev. B*, 61 (2000), 913.
 - [115] R. Madec, B. Devincere, L.P. Kubin, in: L.P. Kubin, et al. (Eds.), *Multiscale Modeling of Materials-2000*, Materials Research Society, Warrendale, PA, 2001.
 - [116] V.V. Bulatov, M. Rhee, W. Cai, in: L.P. Kubin, et al. (Eds.), *Multiscale Modeling of Materials-2000*, Materials Research Society, Warrendale, PA, 2001.
 - [117] M. Rhee, J.S. Stolken, V.V. Bulatov, T. Diaz de la Rubia, H.M. Zbib, J.P. Hirth, *Mat. Sci. Eng. A*, 309-310 (2001), 288.
 - [118] H. Yasin, H.M. Zbib, M.A. Khaleel, *Mat. Sci. Eng. A*, 309-310 (2001), 294.
 - [119] D. Weygand, L.H. Friedman, E. Van der Giessen, A. Needleman, *Modelling Simul. Mater. Sci. Eng.*, 10 (2002), 437.
 - [120] K.W. Schwarz, *Modelling Simul. Mater. Sci. Eng.*, 11 (2003), 609.
 - [121] X. Han, N.M. Ghoniem, Z. Wang, *Phil. Mag.*, 83 (2003), 3705.
 - [122] W. Cai, V.V. Bulatov, J. Chang, J. Li, S. Yip, *Phil. Mag.*, 83 (2003), 539.
 - [123] L.M. Brown, *Phil. Mag.*, 10 (1964), 441.
 - [124] A.G. Khachaturyan, in: E.A. Turchi, R.D. Shull, A. Gonis (Eds.), *Science of alloys for the 21st Century*, TMS Proceedings of a Hume-Rothery Symposium, TMS, 2000, p.293.
 - [125] Y.U. Wang, Y.M. Jin, A.M. Cuitino, A.G. Khachaturyan, *Acta Mater.*, 49 (2001), 1847.
 - [126] Y.M. Jin, A.G. Khachaturyan, *Phil. Mag. Lett.*, 81 (2001), 607.
 - [127] C. Shen, Y. Wang, *Acta Mater.*, 51 (2003), 2595.
 - [128] Y.U. Wang, Y.M. Jin, A.G. Khachaturyan, *Acta Mater.*, 51 (2003), 4209.
 - [129] C. Shen, Y. Wang, *Acta Mater.*, 52 (2004), 683.
 - [130] Y. Xiang, D.J. Srolovitz, L.T. Cheng, W. E, *Acta Mater.*, 52 (2004), 1745.
 - [131] Y. Xiang, D.J. Srolovitz, in: S. Yip (Ed.), *Handbook of Materials Modeling*, Vol.1, Methods and Models of Materials Modeling, Springer, 2005, p.2307.
 - [132] Y. Xiang, D.J. Srolovitz, Dislocation climb effects on particle bypass mechanisms, *Phil. Mag.*, accepted for publication.
 - [133] S.S. Quek, Y. Xiang, Y.W. Zhang, D.J. Srolovitz, C. Lu, Level set simulation of dislocation dynamics in thin films, *Acta Mater.*, accepted for publication.
 - [134] S. Osher, J.A. Sethian, *J. Comput. Phys.*, 79 (1988), 12.
 - [135] P. Burchard, L.T. Cheng, B. Merriman, S. Osher, *J. Comput. Phys.*, 170 (2001), 720.
 - [136] S. Osher, C.W. Shu, *SIAM J. Numer. Anal.*, 28 (1991), 907.
 - [137] G.S. Jiang, D. Peng, *SIAM J. Sci. Comput.*, 21 (2000), 2126.

- [138] C.W. Shu, S. Osher, *J. Comput. Phys.*, 77 (1988), 439.
- [139] R.J. Spiteri, S.J. Ruuth, *SIAM J. Numer. Anal.*, 40 (2002), 469.
- [140] M. Sussman, P. Smereka, S. Osher, *J. Comput. Phys.*, 114 (1994), 146.
- [141] D. Peng, B. Merriman, S. Osher, H.K. Zhao, M. Kang, *J. Comput. Phys.*, 155 (1999), 410.
- [142] S. Osher, L.T. Cheng, M. Kang, H. Shim, Y.H.R. Tsai, *J. Comput. Phys.*, 179 (2002), 622.
- [143] H.K. Zhao, T. Chan, B. Merriman, S. Osher, *J. Comput. Phys.*, 127 (1996), 179.
- [144] S. Chen, M. Merriman, S. Osher, P. Smereka, *J. Comput. Phys.*, 135 (1997), 8.
- [145] D. Adalsteinsson, J.A. Sethian, *J. Comput. Phys.*, 148 (1999), 2.
- [146] Y.H.R. Tsai, L.T. Cheng, S. Osher, H.K. Zhao, *SIAM J. Numer. Anal.*, 41 (2003), 673.
- [147] H.K. Zhao, *Math. Comp.*, 74 (2005), 603.
- [148] E. Orowan, in: *Symposium on Internal Stress in Metals and Alloys*, The Institute of Metals, London, 1948, p.451.
- [149] M.F. Ashby, *Acta Metall.*, 14 (1966), 679.
- [150] P.B. Hirsch, *J. Inst. Met.*, 86 (1957), 13.
- [151] N.F. Mott, F.R.N. Nabarro, *Proc. Phys. Soc.*, 52 (1940), 86.
- [152] J.D. Eshelby, in: F. Seitz, D. Turnbull (Eds.), *Solid State Physics*, Vol 3, Academic Press, New York, 1956.
- [153] A.P. Sutton, R.W. Balluffi, *Interfaces in Crystalline Materials*, Clarendon Press, Oxford, 1995.